NASA TECHNICAL NOTE

NASA TN D-7453

NASA TN D-7453

EXPERIMENTAL STUDIES OF HYPERSONIC BOUNDARY-LAYER TRANSITION AND EFFECTS OF WIND-TUNNEL DISTURBANCES

by P. Calvin Stainback, Richard D. Wagner, F. Kevin Owen, and Clifford C. Horstman

Langley Research Center
Hampton, Va. 23665

NATIONAL AERONAUTICS AND SPACE ADMINISTRATION • WASHINGTON, D. C. • MARCH 1974

For sale by the National Technical Information Service, Springfield, Virginia 22151

1. Report No.	2. Government Accession No.	3. Recipient's Catalog No.
NASA TN D-7453		

4. Title and Subtitle	5. Report Date
EXPERIMENTAL STUDIES OF HYPERSONIC BOUNDARY-LAYER TRANSITION AND EFFECTS OF WIND-TUNNEL DISTURBANCES	March 1974
	6. Performing Organization Code

7. Author(s)	8. Performing Organization Report No.
P. Calvin Stainback and Richard D. Wagner, Langley Research Center F. Kevin Owen and Clifford C. Horstman, Ames Research Center	L-9154

9. Performing Organization Name and Address	10. Work Unit No.
NASA Langley Research Center Hampton, Va. 23665	501-06-07-03
	11. Contract or Grant No.
	13. Type of Report and Period Covered
	Technical Note
12. Sponsoring Agency Name and Address	14. Sponsoring Agency Code
National Aeronautics and Space Administration Washington, D.C. 20546	

15. Supplementary Notes

16. Abstract

Boundary-layer transition data on cones and free-stream disturbance levels were measured in the Ames 3.5-foot hypersonic wind tunnel and the Langley Mach 8 variable-density hypersonic tunnel. Transition data were obtained by using different conical models and techniques for detecting the location of transition. The disturbance levels were measured by using hot-wire anemometry and pressure transducers. The transition Reynolds numbers obtained from the tests at the Ames Research Center correlated well with other transition data obtained in similar facilities at the Langley Research Center when the fluctuating pressures measured at the surface of conical models were used as a correlating parameter.

17. Key Words (Suggested by Author(s))	18. Distribution Statement
Boundary-layer transition Wind-tunnel disturbances Transition correlation	Unclassified – Unlimited STAR Category 12

19. Security Classif. (of this report)	20. Security Classif. (of this page)	21. No. of Pages	22. Price
Unclassified	Unclassified	46	$3.00

EXPERIMENTAL STUDIES OF HYPERSONIC BOUNDARY-LAYER TRANSITION AND EFFECTS OF WIND-TUNNEL DISTURBANCES

By P. Calvin Stainback and Richard D. Wagner
Langley Research Center

F. Kevin Owen* and Clifford C. Horstman
Ames Research Center

SUMMARY

Boundary-layer transition data on cones and free-stream disturbance levels were measured in the Ames 3.5-foot hypersonic wind tunnel and the Langley Mach 8 variable-density hypersonic tunnel. Transition data were obtained by using different conical models and techniques for detecting the location of transition. The disturbance levels were measured by using hot-wire anemometry and pressure transducers. The transition Reynolds numbers obtained from the tests at the Ames Research Center correlated well with other transition data obtained in similar facilities at the Langley Research Center when the fluctuating pressures measured at the surface of conical models were used as a correlating parameter.

INTRODUCTION

The transition of boundary layers from a laminar to a turbulent state can have a pronounced effect on the performance of aircraft and missiles. Therefore, a knowledge of the location of transition is important for design purposes. However, transition is a very complex process, and the many theoretical and experimental studies that have been conducted for the purpose of predicting the location of transition have not, in general, been successful. For theoretical studies, the necessary simplifying assumptions required to make the mathematics tractable preclude the application of these results to practical design problems. Even though there is a vast amount of experimental data available for the location of transition, the complexity of transition and the lack of fully documented test conditions make it difficult to utilize these data for making predictions.

---

*Visiting Associate Professor, University of Santa Clara, Santa Clara, Calif. (Consultant at NASA Ames Research Center).

The reason for the complexity of the transition process is twofold. First, the profiles of the laminar boundary layer that determine the stability of the boundary layer depend on many variables – some of which are difficult to control in the test environment. Second, disturbances introduced into the laminar boundary layer alter the profiles and promote transition. These disturbances may be introduced from the surface of vehicles and models and from the free stream. Often these disturbances cannot be controlled, and frequently they are not considered when transition data are obtained and analyzed.

As a result of these two problems, transition data obtained with a flight vehicle or a model in a given facility often do not agree with data obtained with another vehicle or model in a second facility even though the profiles of the laminar boundary layer and the disturbances are ostensibly similar. The discrepancies between transition data are greatest for measurements made in conventional wind tunnels. These discrepancies are probably due to the fact that there are considerably more data available from these facilities than from flight or other types of facilities. Therefore, in order for transition data obtained in conventional wind tunnels to be useful, some method must be found for correlating these data to reduce the discrepancies to a satisfactory level. The satisfactory extrapolation of data taken in wind tunnels to flight conditions is desirable; however, this cannot be expected until the successful correlation of wind-tunnel data is achieved.

Recent results obtained at high supersonic and hypersonic speeds indicate that much of the discrepancy between transition data taken in wind tunnels can be attributed to the differences in the disturbance levels in the free stream (refs. 1 to 5). In a properly designed tunnel, the predominant disturbances have been shown to be aerodynamic noise generated by the turbulent boundary layer on the nozzle wall (ref. 6). Quantitative data supporting this concept were first published in reference 3. In these studies (ref. 3), the disturbance levels were measured with a hot-wire anemometer. Recently, pressure transducers and hot-wire anemometers have been used to determine the level of the free-stream disturbances and have successfully related these levels to the location of transition (refs. 4 and 5).

It is the purpose of this paper to report further investigations on the effect of disturbance levels on the locations of transition obtained on sharp cones at hypersonic speeds. Two facilities were used in this investigation: the Ames 3.5-foot hypersonic wind tunnel and the Langley Mach 8 variable-density hypersonic tunnel. These two tunnels, though different in certain aspects, were thought to be sufficiently similar to give comparable results for the location of transition on similar models. Transition data obtained in the past, however, indicated that there were considerable differences in transition data measured in these facilities (ref. 7). These differences prompted the present investigation to resolve, if possible, the discrepancies between the two sets of data. New transition data were obtained in both facilities by using several conical models. The dis-

turbance levels in the two facilities were measured by using both hot-wire anemometry and pressure transducers. Pressure transducers were used to measure the fluctuating pitot pressures and fluctuating pressures at the surface of a conical model.

The description and calibration of the instrumentation used in this investigation is included in an appendix.

SYMBOLS

A_w' overheat parameter

a,b,c constants in figure 3

c heat capacity of wire

d diameter of wire

E' finite-circuit parameter

e electrical potential

Δe unsteady voltage across wire

h heat-transfer coefficient

I mean current through wire

$K = \frac{d \log R_w}{d \log T_w}$

k coefficient of thermal conductivity

M_e local Mach number

M_∞ free-stream Mach number

m mass flow rate

$\mathscr{M}$ wire time constant

N_{Nu} Nusselt number

N_{Re} unit Reynolds number

$N_{Re,s}$ local Reynolds number based on surface distance from apex

N_{St} Stanton number

p pressure

R resistance of wire

$R_{mT} = \dfrac{\overline{m' T_t'}}{\tilde{m} \tilde{T}_t}$

$r = \dfrac{\Delta e_m}{\Delta e_T}$

T temperature

V mean voltage across wire

α linear coefficient of resistivity

γ nonlinear coefficient of resistivity

ϵ finite circuit factor

η recovery factor

θ_c cone half-angle

$\tau_{w,r}$ temperature loading of wire, $\dfrac{T_w - T_r}{T_r}$

Subscripts:

b beginning

c surface conditions on cone

e end

m	mass flow
r	recovery
ref	reference
s	surface distance from apex
T	total temperature
t	total conditions
tr	transition
w	wire
2	behind normal shock
∞	free-stream conditions

A prime (') with a symbol indicates instantaneous; a tilde (~) over a symbol indicates rms of fluctuating quantities; and a bar ($\bar{}$) over a symbol indicates time average value.

DESCRIPTION OF FACILITIES

Ames 3.5-Foot Hypersonic Wind Tunnel

A sketch of the original Ames 3.5-foot hypersonic wind tunnel (Ames HWT) – called version A – is shown in figure 1(a). The tunnel was of the blowdown type, and high pressure air was heated in a pebble-bed heater. The upper end of the heater, above the pebbles, served as a settling chamber for the nozzle. There were no screens or baffles in the heater (the settling chamber) or in the inlet approach to the nozzle. An annular slot was located upstream of the throat of the nozzle, and air or helium was injected into the flow to provide insulation between the nozzle wall and the hot airstream.

The nozzle was axisymmetric and designed to give a uniform flow at the exit. The nozzle was 6.1 m long from the throat to the exit, and a conventional cylindrical test section, 1.066 m in diameter, was located at the exit of the nozzle. An injection mechanism was used to insert models into the test section after steady flow conditions were established. The maximum length of models that could be injected was 1.0 m.

Air could be supplied to the tunnel at pressures from 100 to 1250 N/cm^2 and the temperature of the air could range from 700 to 1900 K.

The original tunnel, version A, was altered to version B after April 1972. The major changes were made in the heater and test section. (See fig. 1(b).) The pebbles in the heater were replaced with bricks having passages that were alined when the bricks were properly stacked. The passages formed were 6 mm in diameter and 6.4 m long. In version B, a test cabin replaced the test section and tests were made in a free jet. An injection mechanism was located in the test cabin for inserting models into the jet.

After the alteration, only air was used as an insulating medium for the throat of the nozzle.

The Mach number of the jet ranged from 7.25 to 7.32 for pressures from 100 to 1200 N/cm^2, respectively. The test core was approximately 0.7 m in diameter with an axial Mach number gradient less than 0.12/m.

Langley Mach 8 Variable-Density Tunnel

A sketch and photograph of the Langley Mach 8 variable-density tunnel (Langley VDT) are presented in figures 2(a) and 2(b), respectively. High pressure air is heated in an electric heater. Cold air enters the bottom of the heater and flows to the top of the heater outside tubes that are arranged in several bundles. The air then flows down the inside of the heated tubes and exhausts through a 12.7-cm pipe at the bottom of the heater. There is a system of pipes and valves between the heater and the settling chamber (fig. 2(c)). In version A of this facility, valves A and B were 12.7 and 5.1 cm, respectively.

The settling chamber was about 1.5 m long and about 0.35 m in diameter. For version A, screens and baffles in the settling chamber consisted of a perforated conical baffle at the entrance of the settling chamber followed by a set of three screens. Each screen was fabricated with two pieces of wire screen. The first was of 50-mesh screen with a wire diameter of 0.2 mm; the second was of 4-mesh screen with a wire diameter of 1.5 mm. The 4-mesh screen was placed downstream of the 50-mesh screen for support. (See fig. 2(a).) The first screen was mounted about 0.1 m downstream of the inlet baffle and the screens were about 0.1 m apart. A second set of screens, identical to the first set, was located about 0.81 m downstream of the first set. The distance from the last screen, in this second set, to the throat of the nozzle was 0.4 m.

The nozzle was 2.7 m long from the throat to the test section, and the diameters of the throat and test section were 1.47 cm and 0.46 m, respectively. An injection system was used to insert models into the test section after steady flow conditions were established. The maximum model length that could be injected was about 0.7 m.

The Mach number in the test section was a function of the stagnation pressure and varied from about 7.2 to 8.1 over the large range of pressures at which the tunnel could operate. A Mach number calibration curve for the tunnel is presented in figure 3. The total temperature of the air is also a function of the total pressure as a result of decreased heater efficiency and heat losses to pipes and valves at low mass flows. Generally, the total temperature ranged from about 700 K at low pressures (20 N/cm^2) to 810 K at high pressures (2000 N/cm^2).

The major differences between versions A and B of this facility are the control valves for the high pressure air to the settling chamber and the system of screens in the settling chamber. In version B, valve A was replaced with a 10.2-cm valve. For some tests to be described, valve A was removed from the system and blank flanges were substituted for the valve. This alteration of the tunnel will be referred to as version B-1.

A sketch of the screens in the settling chamber for version B is shown in figure 2(a). The major difference between the screens for the two versions of the tunnel is the substitution of a thick porous plate having a large pressure drop for conventional wire screens and the increase in distance from the last screen to the inlet of the nozzle. A porous plate, 0.4 cm thick, was located 0.1 m downstream of the inlet baffle. The pressure drop across the plate was 35 N/cm^2 when the mass flow of air was 20 kg/sec. A structure was mounted downstream of the porous plate to support the plate during initiation of flow since transient conditions could cause an increase in the pressure drop across the plate. A 50-mesh screen with wire diameter of 0.9 mm was mounted about 10 cm downstream of the porous plate and support. A second screen identical to the first was located 25 cm downstream from the first. The distance from the second screen to the entrance of the nozzle was about 1.0 m.

DESCRIPTION OF MODELS AND TEST METHODS

Four models were used during the present tests and each model was tested in version B of each wind tunnel. The models were as follows: a thin-film model for obtaining hot-film anemometer data, two thermocouple models for measuring heating rates, and a pressure model for measuring fluctuating pressures at the surface of a cone.

Thin-Film Model

The thin-film model was a 5^o half-angle cone machined from a solid billet of steel. Five platinum thin-film gages were mounted on glass inserts and installed flush with the model surface at distances between 20.3 and 61.0 cm from the apex of the cone (fig. 4). The transition measurements were made by using a quick insert mechanism and the model was never exposed to the hot airstream for more than 15 seconds. The change in the wall temperature during the test was negligible. The instantaneous change in temperature of

the thin-film gages was monitored with a constant temperature anemometer that had a frequency response of 20 kHz. The root mean square of the output of the anemometer was used to detect transition.

Thermocouple Models

One thermocouple model was a 5° half-angle cone machined from several pieces of steel and joined as shown in figure 4. The two most forward pieces, the nose and transition piece, had a uniform wall that was nominally 0.762 mm thick. The body of the cone was 0.635 cm thick and had a slender wedge-shape insert forming part of the conical surface. This piece was 0.762 mm thick. The afterbody of the cone was 0.762 mm thick and was fitted over an aluminum mandrel for support. The mandrel was also used to support the body of the model and to attach the model to a strut. The various parts of the model – the nose, transition piece, body, and afterbody – were instrumented with iron-constantan thermocouples. The spacing for the thermocouples was about 0.635 cm.

For tests in the Ames HWT, the mandrel and strut were replaced by a mandrel and sting.

The second model was a 16° half-angle cone with a uniform wall that was 0.762 mm thick. The model was mounted on a sting that fitted into the nose and base of the model (fig. 4(b)). The model was instrumented with 86 iron-constantan thermocouples located about 2.54 mm apart.

The testing technique for the thermocouple models was typical of the transient calorimeter method. The heat-transfer rates were calculated from temperature-time histories about 1/2 sec after the model was injected into the test stream.

16° Conical Pressure Model

The pressure model (fig. 4(b)) was machined from a solid billet of aluminum and bored to receive two pressure transducers and an accelerometer. The fluctuating pressure data were obtained by injecting the model into the test section after steady-state conditions were established. Data were taken for about 15 sec.

METHOD FOR DETERMINING THE LOCATION OF TRANSITION

Three values for the "transition" Reynolds number can be defined for the data obtained with the thin-film gages (ref. 8). (See sketch a.) The lowest of these values is defined as the "onset of transition" and occurs when the rms voltage from the thin-film gage first increased from its laminar value, that is, where intermittency begins and can be clearly seen on an oscilloscope. This is the only value of the transition Reynolds number used herein. When thermocouples are used to determine the transition Reynolds

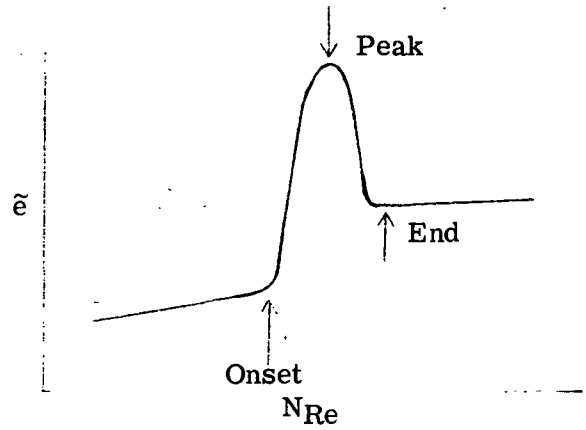

Sketch a

numbers, there are four values of the Reynolds number that can be defined as illustrated in sketch b. The onset of transition is defined as the Reynolds number where the meas-

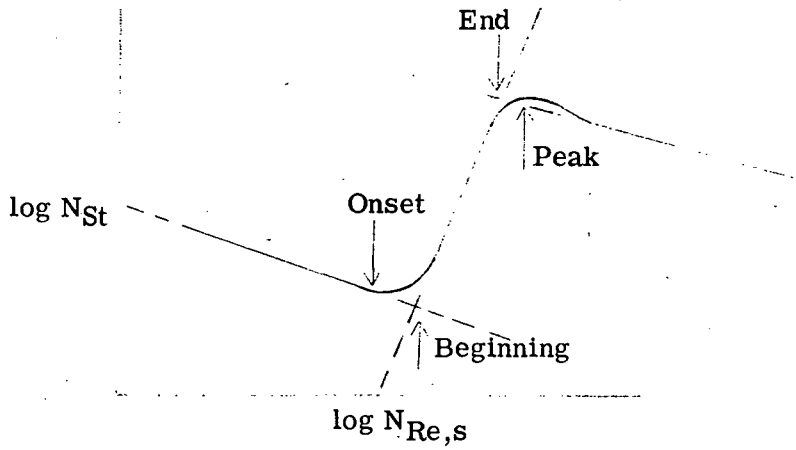

Sketch b

ured Stanton numbers first consistently exceed the laminar value and represents the lowest transitional Reynolds number that can be obtained from heat-transfer data. The "beginning" of transition was obtained by fairing straight lines through the laminar and transitional data. The beginning of transition is determined by the intersection of these lines. Most of the transition data presented represent the beginning of transition. Some of the data represent the onset of transition.

The transition Reynolds numbers obtained using the two techniques (hot film and thermocouple) are not, in general, comparable. However, the onset of transition obtained with the two methods should tend to agree. The thin-film technique would probably indicate a lower value since this technique is sensitive to instantaneous changes in the local heating rates.

REVIEW OF DATA TAKEN IN VERSION A OF AMES HWT AND LANGLEY VDT

Transition data measured on models in version A of the Ames HWT and the Langley VDT will be presented to illustrate the discrepancies between the transition Reynolds numbers measured in the two facilities. Most of these data were measured using a 5^{o} cone and have been published previously. Some data for conical models having other half-angles are presented to further illustrate the difference between the transition Reynolds numbers measured in versions A and B of the Langley VDT. These data are presented in table I(a).

Transition data measured on a 5^{o} half-angle cone in version A of the Ames HWT was reported in reference 7. These data are shown in figure 5 along with transition data measured on two different 5^{o} half-angle cones in version A of the Langley VDT. Transition data taken on a model cast from a high-temperature epoxy and using temperature-sensitive paints were reported in reference 9. The other data from the Langley VDT were obtained on the 5^{o} half-angle cone shown in figure 4(a). The data obtained in the Langley VDT with the two different models agreed fairly well. There is a significant variation of the transition Reynolds number with unit Reynolds number; the slopes of a straight line faired through the data (least-square method) obtained on the thermocouple and paint models were 0.31 and 0.39, respectively. The transition data from the Ames HWT had only a slight variation with unit Reynolds number (slope equal to 0.13) and the level of the data is significantly higher than those obtained in the Langley VDT. The difference is greatest at the lower unit Reynolds numbers where the values of $N_{Re,s,tr}$ from the Ames HWT are approximately twice those obtained in the Langley VDT.

Transition data were measured on other thermocouple models in version A of the Langley VDT and an example of these data is shown in figure 6. The values of the transition data for the 10^{o} and 16^{o} cones are almost identical, and a straight line faired through the data would have a slope of about 0.45. A comparison of the transition data from figures 5 and 6 shows that there is little difference in the level of the transition Reynolds numbers for the various models even though the local Mach number ranged from 5 for the 16^{o} cone to 7.24 for the 5^{o} cone. A comparison of these results with data obtained in the Langley 22-inch helium and the Langley Mach 20 high Reynolds number helium tunnels is shown in figure 7. The figure shows that transition Reynolds numbers measured in version A of the Langley VDT is about the same in the range of $5 \leqq M_e \leqq 7.24$. The variation that can be observed in figure 7 is opposite from the one reported in reference 4. This apparent invariance of the transition Reynolds number with local Mach number has been previously reported in reference 9 for conical models having different half-angles. The reason for this lack of dependence of $N_{Re,s,tr}$ on M_e is

not understood at the present time since the levels of $\tilde{p}_e/\bar{p}_e$ would be very nearly the same and a change in M_e would be expected to change $N_{Re,s,tr}$ (ref. 4).

TRANSITION DATA TAKEN IN VERSION B OF AMES HWT AND LANGLEY VDT AND COMPARISON WITH DATA TAKEN IN VERSION A

Transition data (representing the beginning of transition) taken on two different 5^o conical models in versions A and B of the Ames HWT are presented in figure 8. The data for version B are tabulated in table I(b). The data obtained in version B of the tunnel with two different models and different measuring techniques tend to agree. The present data are somewhat lower than the previous data with the greatest discrepancy being at the lower unit Reynolds numbers. Initially it was thought that differences between the previous and present data were due to the difference in the measuring techniques, that is, the use of thin-film gages versus thermocouples. However, the present data obtained by the two techniques agree.

The alteration of the facility could affect the location of transition measured on models; however, previous data (ref. 10) taken in version A of the tunnel by using the model instrumented with thin-film gages (not shown in fig. 8) agreed with the present data obtained on the same model. The only difference in the tunnel for the two tests was the gas used for insulating the throat from the hot air. The data from reference 7 were obtained with helium as the insulating gas; the other data were obtained with air as the insulating gas.

The transition data obtained in versions A and B of the Langley VDT on a 5^o conical model are presented in figure 9. The data for version B are tabulated in table I(b). The transition Reynolds numbers taken in version B are significantly greater than those taken in version A for the unit Reynolds numbers of the investigation. The increase was fairly uniform over the range of unit Reynolds numbers. The onset of transition determined from the thin-film gages occurred at transition Reynolds numbers that are somewhat lower than the data obtained from thermocouples. These results indicate a significant reduction in the disturbance level for version B of the Langley VDT. This reduction is attributed to the improved screen configuration in version B of the tunnel. (See fig. 2(a).) For example, the 0.64-cm-thick Rigimesh screen is probably sufficiently thick and impermeable to eliminate total temperature fluctuation in the free stream that could be present due to faulty mixing at the exit of the heater. The large pressure drop across the Rigimesh screen would also reduce the possibility of flow separation in the entrance cone.

The data for the various 5^o conical models are presented in figure 10 for version B of the two tunnels. The beginning of transition measured in the Langley VDT appears to

be higher than the other data by a few percent. At low unit Reynolds numbers, the heat-transfer data obtained in the Langley VDT with the 5° conical model instrumented with thermocouples had an anomalous behavior similar to that noticed by Softley and reported in reference 11. That is, there is an initial deviation of the heat-transfer data from the laminar values, but the deviation is not as great as generally found for heating rates in the transition region as illustrated in figure 11. Therefore, the present method for defining the beginning of transition would result in the transition Reynolds numbers being high. Also shown in figure 10 is the onset of transition as determined from the thermocouple data in the Langley VDT. With these data, the transition Reynolds numbers agree within ± 15 percent for the two tunnels and for the two models.

The transition data measured on the 10° and 16° conical models in versions A and B of the Langley VDT are presented in figure 12. The data for version B are tabulated in table I(b). In general, the transition Reynolds numbers for version B of the tunnel are greater than those for version A, particularly at the lower unit Reynolds numbers. However, the difference between the data taken in version A and version B is not as great for the 10° and 16° models as for the 5° model. (See fig. 9.)

Data taken in version B of the Ames HWT and the Langley VDT with the 16° conical model are presented in figure 13. The lower symbols represent data from the two tunnels when the total temperatures were about the same. For these conditions, the data from the two facilities tended to agree. However, when the Ames HWT was operated at lower total temperatures, well above values required to prevent liquefaction of oxygen in the test section, the transition data were somewhat higher than the data taken at the higher total temperatures. The variation of the transition Reynolds number with total temperature at a constant wall temperature agreed with recent data reported in reference 12 by Mateer.

DISTURBANCE LEVEL MEASUREMENTS

Hot-Wire Anemometer Results From Ames HWT

Three typical mode diagrams of the hot-wire signal in the free stream of the Ames HWT are shown in figure 14(a). The two sets of data at $p_t \approx 113$ are indicative of the fair degree of repeatability of the tests. Within the data scatter, a straight line can be faired through each set of data. Such a fairing implies that $R_{mT} = -1$ and that the slope of the straight line and the $\tilde{e}/\overline{V}\Delta e_T$ intercept (at $r = 0$) give the rms of the mass flow and total-temperature fluctuations, respectively; that is, from equation (A10), since $R_{mT} = -1$,

$$\frac{\tilde{e}}{\overline{V}\Delta e_T} = \frac{\tilde{T}_t}{\overline{T}_t} + \frac{\tilde{m}}{\overline{m}} r \qquad (1)$$

The root mean squares of the mass flow and total temperature fluctuations that were calculated from equation (1) and the mode diagrams are shown for the stagnation pressure range of the tests in figure 14(b). These data are tabulated in table II. The scatter in the data of figure 14(b) is quite large, partly because of the poor signal-to-noise ratio of the recorded signals (which was at most about 8 to 1 at the highest overheats). Also, the environment of the Ames HWT, particularly the high particle density in the stream and the high-temperature blowdown operation, is not conducive to quantitative hot-wire anemometry. In view of the data scatter, no trends in turbulence level with operating pressure could be established and this hot-wire data should be viewed as a "back-up" measurement for the other disturbance measurements made. The average values indicated in figure 14(b) of $\frac{\tilde{m}}{\overline{m}} = 2.65$ percent and $\frac{\tilde{T}_t}{\overline{T}_t} = 0.83$ percent should be adequate as an approximate measure of the disturbance level over the pressure range.

If one assumes that the disturbances sensed by the hot wire are sound waves radiated from the turbulent nozzle wall boundary layers (the hot-wire theory shows this to be an assumption that is consistent with the linear mode diagrams), then the pressure fluctuation levels can be calculated as shown in reference 3. The results of these calculations are shown in table II. The pressure fluctuation level is quite high; the average value is about 4 percent. If sound is not the only disturbance mode present, these calculated values of $\tilde{p}_\infty/\overline{p}_\infty$ would be too large. Most likely there is an additional mode present – temperature spottiness due to nonuniform heating of the supply gas. The high $\tilde{T}_t/\overline{T}_t$ values obtained suggest that the temperature spottiness is present since, in tests performed in unheated helium tunnels (without temperature spottiness), the $\tilde{m}/\overline{m}$ values are typically two orders of magnitude larger than the $\tilde{T}_t/\overline{T}_t$. Thus, the pressure levels indicated in table II should be viewed as an upper bound on the actual $\tilde{p}_\infty/\overline{p}_\infty$.

Pressure Transducer Results From Ames HWT

The fluctuating pitot pressures and the fluctuating surface pressures measured on the 16° cone are presented in figure 15 and in tables III(a) and IV(a). The fluctuating pressures calculated by using the hot-wire data are also presented in the figure. A description of the pressure measuring system is included in the appendix.

The nondimensionalized disturbances obtained with the pitot probe and the conical model agreed very well over the test range of unit Reynolds number. However, the average disturbance level measured with the hot-wire anemometer was about twice those measured with the pressure transducers. This result is contrary to those reported in reference 13. In this reference, hot-wire data and fluctuating pitot pressures were measured at Mach 5 in air and Mach 20 in helium. For these tests (ref. 13), the normalized fluctuating pressures measured with pitot probe were about twice those calcu-

lated from the hot-wire data. An explanation for these differences is not available at the present time.

Pressure Transducer Results From Langley VDT

Fluctuating pressure levels measured on the 16° cone for versions B and B-1 of the Langley VDT are presented in figure 16 and in table III(b). At low unit Reynolds numbers there is a significant difference between the measured disturbance levels. However, at the higher unit Reynolds numbers this difference is negligible. The reason for this change in the disturbance levels is presumably due to the changes in the valves upstream of the settling chamber. The nondimensionalized disturbance levels measured with the pitot probe are also presented in figure 16 and in table IV(b). In general, the normalized fluctuating pitot pressures are about 15 percent below the normalized fluctuating pressures measured at the surface of the 16° cone underneath the laminar boundary layer.

The normalized fluctuating pressures for the two tunnels are compared in figure 17. The disturbance level for the Ames HWT appears to be lower (about 70 percent) than those for the Langley VDT for the test unit Reynolds number range. This result agrees qualitatively with the results published by Pate and Schueler (ref. 1); that is, if everything else is constant, the noise level of high supersonic and hypersonic tunnels decreases with increasing diameter of the nozzle at the test section.

Spectra of the Disturbances

Plots of typical power density spectra are presented in figure 18 for disturbance measurements made with the hot-wire anemometer and the pressure transducers. In general, most of the energy was concentrated at low frequencies for both facilities; however, this tendency was more pronounced for the Ames HWT. Since the Ames HWT is larger than the Langley VDT, this later result would probably be expected. The spectra obtained from measurements made with the hot-wire anemometer and the pitot probe are, in general, monotonically decreasing with increasing frequency. The spectra obtained in both facilities from the surface pressure measurements on the 16° cone show an anomalous variation at about 45 kHz. This was probably due to the rubber that was used to fair the face of the pressure transducer to the contour of the conical surface.

Correlation of Transition Data Using Measured Disturbance Levels

The transition data and the fluctuating pressures measured on the 16° cone in the Ames HWT are compared with other transition and pressure data in figure 19. Figure 19 shows that the transition data from the Ames HWT correlate well with the other data when the local nondimensional fluctuating pressures are used as the correlating parame-

ter. The nominal local Mach number on the conical models for these data was about 5. There are, however, some slight differences in the profile of the laminar boundary layer on these models due to the differences in the local Mach number, wall-to-total enthalpy ratio, and total enthalpy, but these differences are believed to have a negligible effect on the transition Reynolds numbers and the normalized fluctuating pressures.

CONCLUSIONS

Boundary-layer transition locations and disturbance levels were measured in the Ames 3.5-foot hypersonic wind tunnel (Ames HWT) and the Langley Mach 8 variable-density hypersonic tunnel (Langley VDT). Data were taken in two versions of both facilities. The original design of each facility was noted as version A. Certain alterations in each facility were noted as version B. In the Ames HWT, changes were made in the heater and the test section, and air was substituted for helium as the cooling medium for the nozzle. In the Langley VDT, changes were made in the valves upstream of the settling chamber and in the screens in the settling chamber. Transition data were measured by using several different conical models and by using different techniques for detecting the location of transition. The disturbance levels were measured with hot-wire anemometry and pressure transducers. From the results, the following conclusions can be made:

1. The transition Reynolds numbers measured in the original design (version A) of the facilities on 5° conical models instrumented with thermocouples did not agree with those measured in the modified facilities (version B) with similar or identical models.

2. In general, the transition Reynolds numbers measured on a 5° cone in version A of the Ames HWT were higher than those measured in version B. However, the transition Reynolds numbers measured in version A of the Langley VDT were lower than those measured in version B. The discrepancies between the data from both tunnels were larger at the lower unit Reynolds numbers.

3. The transition Reynolds number measured on two 5° cones in versions B of the Ames HWT and the Langley VDT were in good agreement.

4. The transition Reynolds numbers measured in version B of the Ames HWT on a 16° cone agreed well with those measured on the same model tested in version B of the Langley VDT when the total temperatures were about equal. At lower total temperatures, the transition Reynolds numbers obtained in the Ames HWT were larger than the ones obtained at higher total temperatures.

5. The disturbances measured in version B of the Ames HWT using pressure transducers indicated that the fluctuating pressures normalized by the local pressure were about 70 percent of those measured in version B of the Langley VDT.

6. The rms fluctuating pressures measured in version B of each tunnel, using a pitot probe and a flush mounted pickup on a 16^{o} cone, had about the same values when the levels were nondimensionalized by the local mean pressures. In the Langley VDT the normalized fluctuating pitot pressures were somewhat below the fluctuating pressures measured at the surface of a 16^{o} cone.

7. The transition Reynolds numbers measured in version B of the Ames HWT correlated well with data taken in several wind tunnels at the Langley Research Center when the nondimensionalized rms pressure levels measured at the surface of conical models were used as the correlation parameter.

Langley Research Center,
National Aeronautics and Space Administration,
Hampton, Va., January 15, 1974.

APPENDIX

DESCRIPTION AND CALIBRATION OF INSTRUMENTATION

Hot-Wire Instrumentation and Methods

The hot-wire measurements were made with a constant current anemometer with a frequency response up to 500 kHz. However, the data to be presented were filtered above 100 kHz since there was a negligible amount of signal above this frequency and filtering the higher frequencies improved the signal-to-noise ratio. The hot-wire probe (fig. 20) consisted of two needles, embedded in a wedge-shaped holder, which supported the wire that was the sensing element of the probe. The holder was cast from a high-temperature epoxy with the needle tips spaced about 0.175 cm apart. Nickel plated, platinum wire was silver soldered across the tips of the needles, and a length (centered about midspan) of about 0.076 cm was etched to remove the nickel plating. The etched, platinum wire (the sensing portion of the wire) was 5.08 μm in diameter. About a quarter circle slack was formed in the wire to help avoid "strain-gage" effects in the signals. The wire was checked for strain-gage oscillations in a small hypersonic helium nozzle which has sufficient turbulence to excite strain-gage oscillations, and no oscillations were found. The measurements to be discussed were all made with this single probe and a single wire. The wire was temperature calibrated at low temperatures (up to 420 K) to determine its temperature-resistivity coefficient α_{ref} defined by the relation

$$R_w = R_{ref}\left\{1 + \alpha_{ref}(T_w - T_{ref}) + \gamma_{ref}\left[\alpha_{ref}(T_w - T_{ref})\right]^2\right\} \tag{A1}$$

The value of α_{ref} was 0.0038 per K which agrees with the value suggested in reference 14. The temperature calibration facilities were not adequate to determine the nonlinear temperature-resistivity coefficient γ_{ref}, and the value suggested in reference 14 was used, that is, $\gamma_{ref} = 0.045$.

The heat-loss and recovery-factor calibration for the wire was obtained as part of the tests in which the turbulence level was measured in the Ames 3.5-foot hypersonic wind tunnel; that is, the wire Nusselt number

$$N_{Nu,T} = \frac{hd}{k_T} = \frac{I^2 R_w}{\pi \ell k_T (T_w - T_r)} \tag{A2}$$

and the recovery factor

$$\eta = \frac{T_r}{T_{t,\infty}} \tag{A3}$$

(where T_r is the wire resistance with no current and l is the wire length) were determined by recording the mean wire voltage at several currents for each stagnation pressure. The stagnation pressure was limited to 600 N/cm^2 in the tests because exploratory tests showed that the wires would break due to loading at higher pressures. The Nusselt number calibration is shown in figure 20. A good fit to the data is

$$N_{Nu,T} = 0.06 + 0.55\sqrt{N_{Re,T}} \tag{A4}$$

The recovery factor was nearly constant at $\eta = 0.94$.

In addition to the heat-loss and recovery-factor calibrations, the heat capacity of the wire was determined from tests performed in the small helium nozzle previously mentioned. The procedure that was used is outlined in reference 3. The wire time constant $\mathscr{M}$ was measured over a wide range of flow conditions and the heat capacity c was taken as the average value calculated by using the equation

$$\mathscr{M} = \frac{c}{\alpha_r R_r}\left(1 - 2\gamma_r \frac{R_w - R_r}{R_r}\right)\frac{A_w'}{I^2\left(1 + 2A_w'\epsilon\right)} \tag{A5}$$

Since the measurements in the helium nozzle were at low wire temperatures (the stagnation temperature of the helium flow was about room temperature), the value of c, so obtained, was scaled with the specific heat of the platinum to the temperature levels of the tests in the Ames HWT; that is, the measured heat capacity was increased about 5 percent to account for the higher temperature of the air tests. This higher heat capacity was then used to determine the time constants of the wire for the flow conditions in the Ames HWT. For each fluctuation measurement one time constant was used at all overheats; the rms voltage that was recorded was then corrected by using the equation (ref. 3)

$$\frac{\tilde{e}_{true}}{\tilde{e}_{meas}} = \frac{\mathscr{M}_{true}}{\mathscr{M}_{meas}} \tag{A6}$$

For the fluctuation measurements, the basic hot-wire equation for the sensitivity of the hot wire to mass flow and total temperature fluctuations is

$$\frac{e'}{\overline{V}} = \Delta e_T \frac{T_t'}{\overline{T}_t} - \Delta e_m \frac{m'}{\overline{m}} \tag{A7}$$

where e', T_t', and m' are the instantaneous fluctuations in wire voltage, total temperature, and mass flow; $\overline{V}$, $\overline{T}_t$, and $\overline{m}$ are the time average values. The wire sensitivities are given by Morkovin (ref. 14) as

$$\Delta e_m = E'\left(A_w' \frac{d \ln N_{Nu,T}}{d \ln N_{Re,T}} - \frac{A_w'}{\tau_{w,r}} \frac{d \ln \eta}{d \ln N_{Re,T}}\right) \tag{A8}$$

and

$$\Delta e_T = E'\left[K + A_w'\left(K - 1.86 + 0.76 \frac{d \ln N_{Nu,T}}{d \ln N_{Re,T}} + \frac{0.76}{\tau_{w,r}} \frac{d \ln \eta}{d \ln N_{Re,T}}\right)\right] \tag{A9}$$

where Mach number independence of $N_{Nu,T}$ and η has been assumed and constants appropriate for air have been used; E' is the finite circuit factor and $\tau_{w,r}$ is the temperature loading $(T_w - T_r)/T_r$.

The mode diagram approach was used to interpret the fluctuating hot-wire voltage. That is, the hot wire was operated at several currents and a "virtual" total temperature fluctuation $\tilde{e}/\overline{V}\Delta e_T$ is recorded at each current, or sensitivity ratio, $r = \frac{\Delta e_m}{\Delta e_T}$. From equation (A7),

$$\left(\frac{\tilde{e}}{\overline{V}\Delta e_T}\right)^2 = \left(\frac{\tilde{T}_t}{\overline{T}_t}\right)^2 - 2r \frac{\tilde{T}_t}{\overline{T}_t} \frac{\tilde{m}}{\overline{m}} R_{mT} + r^2\left(\frac{\tilde{m}}{\overline{m}}\right)^2 \tag{A10}$$

This equation, when evaluated at the various sensitivity ratios (typically 6 to 7 values of r), yields redundant information to extract the three unknowns, T_t, m, and R_{mT}; R_{mT} is the correlation coefficient of the mass flow and total temperature fluctuations and $R_{mT} = \frac{\overline{m'T_t'}}{\tilde{m}\tilde{T}_t}$.

Fluctuating Pressures

Surface fluctuating pressures on a 16° cone.- The surface fluctuating pressures on a 16° cone were measured by using a Kistler Model 606L Pressure Transducer converted to operate in the Piezotron mode. The converted pickup had a pressure resolution of 0.69 N/m^2 and an acceleration sensitivity of less than 6.9 $N/m^2/g$. A thin coating of RTV silicone rubber was used to fair the pressure sensitive surface of the transducer to the surface of the conical model. This was done because it was believed that a thin coating of RTV would have less effect in the frequency response of the transducer than a port and volume. The transducers were calibrated after the rubber was bonded to its pressure sensitive surface.

A schematic diagram of the pressure measuring and recording system is shown in figure 21. The pressure measuring technique was somewhat unconventional. One of the transducers was subjected to the boundary-layer flow, its fluctuations, and vibration of

the model. A second transducer was shielded from the flow and its output was predominantly due to vibrations of the model. This technique was used because the transducers are sensitive to acceleration and because of the low pressure levels being measured. The net rms pressure level was obtained by subtracting the mean-square pressures indicated by the two transducers and taking the square root of the difference. In this manner the effects of acceleration and electronic noise were minimized. In order to do this properly, the output of the two transducers was matched to give identical outputs for a given acceleration level. This was done by varying the sensitivity of the Kistler Model 504D Dual Mode Charge Amplifier. After the sensitivity settings were made, the transducers were then calibrated with a Photocon Research Products Model PC-120 Pressure Calibrator. An example of a typical calibration is shown in figure 22.

A typical oscilloscope record of the output of the two transducers is shown in figure 23. The upper trace shows the output of the transducer exposed to high-frequency pressure fluctuations under the laminar boundary layer. The lower trace shows the output of the covered transducer. This latter signal is dominated by the low frequency vibrations of the model. The rms voltage level for the covered transducer ranged from about 10 to 20 percent of that for the exposed transducer, depending on the Reynolds number. In general the percentage output of the covered transducer was greatest for the lower Reynolds numbers.

Fluctuating pitot pressures.- A drawing of the pitot probe is shown in figure 24. The transducer mounted in the flat face probe was exposed to the flow and its fluctuations. The transducer in the conical probe was shielded from the flow. The output of the covered transducer was predominantly due to vibration of the probe and the support. This vibration was assumed to be the same for both transducers. The output of the two transducers was reduced as outlined in the previous section.

The rms voltage level for the covered transducer ranged from about 5 to 15 percent of that for the exposed transducer, depending on the total pressure of the test. The higher percentages were experienced at the lower total pressures where the outputs of the transducers approach the noise level of the instrumentation.

The fluctuating pitot pressure transducers used were the Kistler model 202A5 quartz piezotron. These transducers have a pressure resolution of 27 N/m^2 and an accleration sensitivity of less than 14 $N/m^2/g$ along the pressure sensitive axis. The natural frequency of the pickup is about 250 kHz. A thin coating of RTV silicone rubber was used to protect the diaphragm of the transducer from high temperatures and from particles in the flow. The transducers were calibrated after the rubber was bonded to its pressure sensitive surface. An example of a calibration curve for one of the transducers is presented in figure 22. The exposed transducer was mounted in the center of the flat end of a cylinder as shown in figure 24. The diameter of the disk was twice the

diameter of the transducer. This design was used to take advantage of the fact that the pressure across the center portion of a flat face cylinder in supersonic flow is almost constant.

REFERENCES

1. Pate, S. R.; and Schueler, C. J.: Radiated Aerodynamic Noise Effects on Boundary-Layer Transition in Supersonic and Hypersonic Wind Tunnels. AIAA J., vol. 7, no. 3, Mar. 1969, pp. 450-457.

2. Pate, S. R.: Measurements and Correlations of Transition Reynolds Numbers on Sharp Slender Cones at High Speeds. AIAA J., vol. 9, no. 6, June 1971, pp. 1082-1090.

3. Wagner, R. D., Jr.; Maddalon, D. V.; and Weinstein, L. M.: Influence of Measured Freestream Disturbances on Hypersonic Boundary-Layer Transition. AIAA J., vol. 8, no. 9, Sept. 1970, pp. 1664-1670.

4. Stainback, P. C.; Fischer, M. C.; and Wagner, R. D.: Effects of Wind-Tunnel Disturbances on Hypersonic Boundary-Layer Transition. Pts. I and II. AIAA Paper No. 72-181, Jan. 1972.

5. Stainback, P. Calvin: Hypersonic Boundary-Layer Transition in the Presence of Wind-Tunnel Noise. AIAA J., vol. 9, no. 12, Dec. 1971, pp. 2475-2476.

6. Laufer, John: Aerodynamic Noise in Supersonic Wind Tunnels. J. Aerosp. Sci., vol. 28, no. 9, Sept. 1961, pp. 685-692.

7. Mateer, George G.; and Larson, Howard K.: Unusual Boundary-Layer Transition Results on Cones in Hypersonic Flow. AIAA J., vol. 7, no. 4, Apr. 1969, pp. 660-664.

8. Owen, F. K.: Transition Experiments on a Flat Plate at Subsonic and Supersonic Speeds. AIAA J., vol. 8, no. 3, Mar. 1970, pp. 518-523.

9. Stainback, P. Calvin (With appendix by P. Calvin Stainback and Kathleen C. Wicker): Effect of Unit Reynolds Number, Nose Bluntness, Angle of Attack, and Roughness on Transition on a 5° Half-Angle Cone at Mach 8. NASA TN D-4961, 1969.

10. Owen, F. K.; and Horstman, C. C.: Hypersonic Transitional Boundary Layers. AIAA J., vol. 10, no. 6, June 1972, pp. 769-775.

11. Softley, Eric J.: Transition of the Hypersonic Boundary Layer on a Cone. Pt. II – Experiments at $M = 10$ and More on Blunt Cone Transition. Tech. Inform. Ser. No. R68SD14 (Contract AF 04(694)-772), Missile & Space Div., Gen. Elec. Co., Oct. 1968. (Available from DDC as AD 842 422.)

12. Mateer, George G.: Effects of Wall Cooling and Angle of Attack on Boundary-Layer Transition on Sharp Cones at $M_{\infty} = 7.4$. NASA TN D-6908, 1972.

13. Stainback, P. C.; and Wagner, R. D.: A Comparison of Disturbance Levels Measured in Hypersonic Tunnels Using a Hot-Wire Anemometer and a Pitot Pressure Probe. AIAA Paper No. 72-1003, Sept. 1972.

14. Morkovin, Mark V.: Fluctuations and Hot-Wire Anemometry in Compressible Flows. AGARDograph 24, Nov. 1956.

TABLE I.- TRANSITION DATA FOR SHARP CONES

(a) Tunnel version A

θ_c, deg	M_∞ (nominal)	M_e (nominal)	T_t, K	T_s/T_t	$N_{Re,s,tr,t}$	$N_{Re,s,tr,e}$	$N_{Re}/\mu m$	Tunnel	Type of model
5	8.00	7.24	747	0.402	1.76×10^6	---------	4.56	Langley VDT	Thermocouple
			764	.393	1.77	4.16×10^6	7.90		
			753	.403	2.40	4.65	11.64		
			755	.402	3.16	5.30	15.34		
			770	.394	3.06	5.70	18.30		
			759	.400	3.13	6.00	11.60		
			753	.412	2.80	6.85	28.84		
			736	.424	3.57	7.63	39.91		
			750	.414	3.42	7.82	39.11		
			807	.415	4.14	7.90	46.20		
			825	.376	3.01	5.58	17.22		
			820	.373	3.08	6.71	24.90		
			842	.377	3.17	7.39	33.40		
				.374	3.45	7.16	39.80		
5	8.00	7.24	750 (nominal)	≈0.40	1.50×10^6		4.15	Langley VDT	Paint
					1.45		4.25		
					1.50		4.25		
					2.00		8.65		
					2.60		17.50		
					2.30		19.20		
					3.30		42.00		
					4.25		45.00		
5	7.40	6.80	700 (nominal)	≈0.43	3.95×10^6		5.78	Ames HWT	Thermocouple
					4.80		7.45		
					3.90		9.68		
					4.23		12.81		
					5.55		12.81		
					4.95		15.76		
					4.50		16.75		
					5.25		20.69		
					4.90		21.68		
					5.50		24.30		
					5.70		29.89		
					5.30		32.84		
					4.40		35.44		
10	8.00	6.21	758	0.390	2.12×10^6	---------	9.31	Langley VDT	Thermocouple
			748	.394	2.53	4.15×10^6	14.21		
			775	.386	2.58	4.56	16.44		
			780	.387	3.24	5.19	21.91		
			770	.397	3.86	6.35	33.92		
			810	.396	4.45	7.05	40.90		
			758	.411	4.79	7.37	56.40		
			820	.367	3.08	5.08	20.42		
			828	.373	3.62	6.00	29.78		
			834	.376	4.25	6.97	40.00		
			758	.410	4.45	7.09	45.26		
			830	.380	4.74	7.42	49.30		
			795	.404	5.22	7.44	62.90		
16	8.00	5.00	770	0.391	2.28×10^6	---------	8.98	Langley VDT	Thermocouple
			774	.390	2.52	---------	12.56		
			768	.397	2.81	---------	16.05		
			748	.407	3.50	---------	21.60		
			775	.398	4.12	6.34×10^6	30.68		
			764	.409	4.77	7.13	42.58		
			780	.407	4.96	7.46	51.35		
			770	.394	5.32	8.47	63.00		
			837	.380	3.32	---------	18.75		
			837	.371	4.04	6.24	27.80		
			835	.381	4.50	6.93	37.50		
			852	.379	4.94	7.25	45.10		
			808	.403	5.54	7.95	57.65		

TABLE I.- TRANSITION DATA FOR SHARP CONES – Concluded

(b) Tunnel version B

θ_c, deg	M_∞ (nominal)	M_e (nominal)	T_t, K	T_s/T_t	Onset $N_{Re,s,tr}$	$N_{Re,s,tr,b}$	$N_{Re,s,tr,e}$	Peak $N_{Re,s,tr}$	$N_{Re}/\mu m$	Tunnel	Type of model
5	8.00	7.24	750 (nominal)	≈0.40	2.30×10^6				3.8	Langley VDT	Thin film
					2.9				5.7		
					3.2		6.50×10^6	5.40×10^6	10.7		
							7.7		15.2		
							9.9	7.4	24.4		
							11.3		37.0		
								5.5	9.0		
					3.3				8.2		
								5.7	14.0		
5	7.40	6.8	835 (nominal)	≈0.40	2.34×10^6				3.8	Ames HWT	Thin film
					2.75				4.5		
					2.85				5.6		
					2.9				7.1		
					2.94				7.2		
					2.6			5.24×10^6	8.6		
					3.0				9.8		
								5.20	10.2		
							8.40×10^6	5.44	13.6		
								6.09	15.0		
							8.22		16.2		
								6.52	21.4		
							9.50		23.3		
								7.75	25.4		
5	8.00	7.24	701		---	3.12×10^6	---	---	4.92	Langley VDT	Thermocouple
			724		2.58×10^6	3.83	---	---	6.84		
			740		2.88	3.92	---	5.80×10^6	8.46		
			752		2.78	3.97	5.35×10^6	5.75	9.65		
			770		2.96	4.10	6.10	6.35	12.14		
			765		3.65	4.50	6.10	6.30	15.37		
			785		3.85	4.45	6.60	7.10	18.72		
			786		4.00	4.59	6.55	7.15	18.55		
			774		4.60	5.05	7.20	7.80	27.52		
			759		---	5.8	8.40	8.65	37.59		
			780		---	6.25	8.30	9.60	44.42		
			718		---	2.92	---	---	4.79		
			782		---	6.55	8.25	---	4.89		
			703		---	3.12	---	---	5.08		
			699		---	3.35	---	---	5.08		
			719		2.65	3.80	5.70	5.80	8.94		
			721		3.05	3.85	5.75	5.85	9.11		
			759		3.18	4.02	6.15	6.30	11.94		
			741		3.20	4.05	6.15	6.40	12.07		
			759		3.74	4.65	6.30	6.50	15.88		
			764		3.48	4.65	6.25	6.50	15.64		
			780		3.82	4.55	6.65	7.15	18.54		
			772		3.79	4.50	6.60	7.15	18.75		
10	8.00	6.21	770			3.75×10^6	---		14.32	Langley VDT	Thermocouple
			771			3.87	5.50×10^6		17.72		
			785			4.06	5.80		21.27		
			775			4.50	6.50		32.71		
			781			4.85	7.15		42.89		
			791			5.25	7.50		50.68		
			768			5.55	8.20		58.35		
16	8.00	5.0	765			3.58×10^6	---		13.61	Langley VDT	Thermocouple
			770			3.95	---		17.19		
			797			4.07	---		19.79		
			776			4.45	6.20×10^6		30.58		
			774			4.85	6.95		40.45		
			776			5.20	7.30		49.22		
			763			5.50	7.80		56.95		
5	7.32		720	0.412		2.34×10^6	---		4.43	Ames HWT	Thermocouple
			726	.405		2.77	5.09×10^6		8.52		
			703	.421		3.17	5.55		13.58		
			675	.438		3.45	6.27		19.28		
			699	.425		3.76	6.48		22.76		
			736	.399		3.91	6.51		29.30		
			659	.460		5.26	8.87		43.54		
16	7.32		703	0.426		5.03×10^6			21.62	Ames HWT	Thermocouple
			772	.382		5.12			22.89		
			712	.418		4.47			26.25		
			636	.359		7.28	10.36×10^6		45.82		
			1052	.276		3.97			18.92		
			1129	.257		3.76			16.93		
			951	.304		4.43			22.66		
			907	.326		4.52			24.76		

TABLE II.- HOT-WIRE DATA FROM AMES 3.5-FOOT HYPERSONIC WIND TUNNEL

$N_{Re,\infty}/\mu m$	$\tilde{m}/\bar{m}$, percent	$\tilde{T}_t/\bar{T}_t$, percent	$\tilde{p}_\infty/\bar{p}_\infty$, percent	T_t, K
3.85	2.20	0.78	3.68	653
3.96	2.20	.78	3.68	644
6.69	2.35	1.14	4.16	617
7.22	2.00	.66	3.30	711
11.44	3.68	.93	5.86	628
15.36	2.95	.78	3.33	658
21.38	3.15	.72	4.95	633

TABLE III.- FLUCTUATING PRESSURE AT SURFACE OF 16° CONICAL MODEL

(a) Ames HWT

$N_{Re,\infty}/\mu m$	$\tilde{p}_c/\bar{p}_c$, percent	T_t, K	T_s/T_t
3.91	2.25	703	≈0.4
7.54	2.24	709	
11.69	2.03	697	
19.32	1.68	701	
14.63	1.83	726	
25.35	1.66	731	
35.5	1.60	697	

(b) Langley VDT

$N_{Re,c}/\mu m$	$N_{Re,\infty}/\mu m$	$\tilde{p}_c/\bar{p}_c$, percent	T_s/T_t
3.30	2.31	4.15	≈0.40
5.45	3.81	3.75	
9.82	6.87	3.29	
13.80	9.65	3.09	
17.30	12.1	2.85	
20.40	14.28	2.76	
32.10	22.45	2.43	
41.50	29.00	2.31	
48.50	33.90	2.33	
54.50	38.10	2.34	

TABLE IV.- FLUCTUATING PITOT PRESSURES

(a) Ames HWT

$N_{Re,\infty}/\mu m$	$\tilde{p}_{t,2}/\bar{p}_{t,2}$, percent	T_t, K
3.48	2.04	765
3.48	2.26	767
6.45	2.16	779
9.66	2.08	783
11.69	1.88	771
16.70	1.75	764
23.90	1.58	754
31.60	1.56	748

(b) Langley VDT

$N_{Re,\infty}/\mu m$	$\tilde{p}_{t,2}/\bar{p}_{t,2}$, percent	T_t, K
0.925	2.57	705
1.438	3.57	694
2.08	3.57	712
3.31	3.31	744
5.01	3.07	727
6.36	2.92	742
8.00	2.84	787
10.52	2.67	791
12.58	2.59	812
18.72	2.34	803
26.15	2.11	807
29.05	1.96	827
35.40	1.81	797

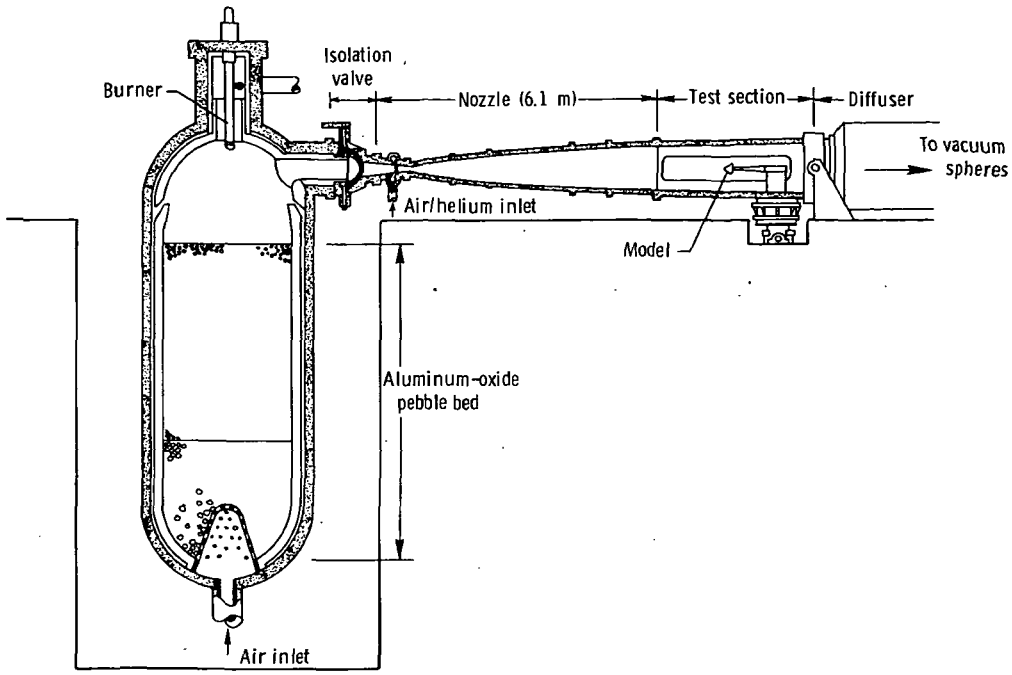

(a) Original design (version A).

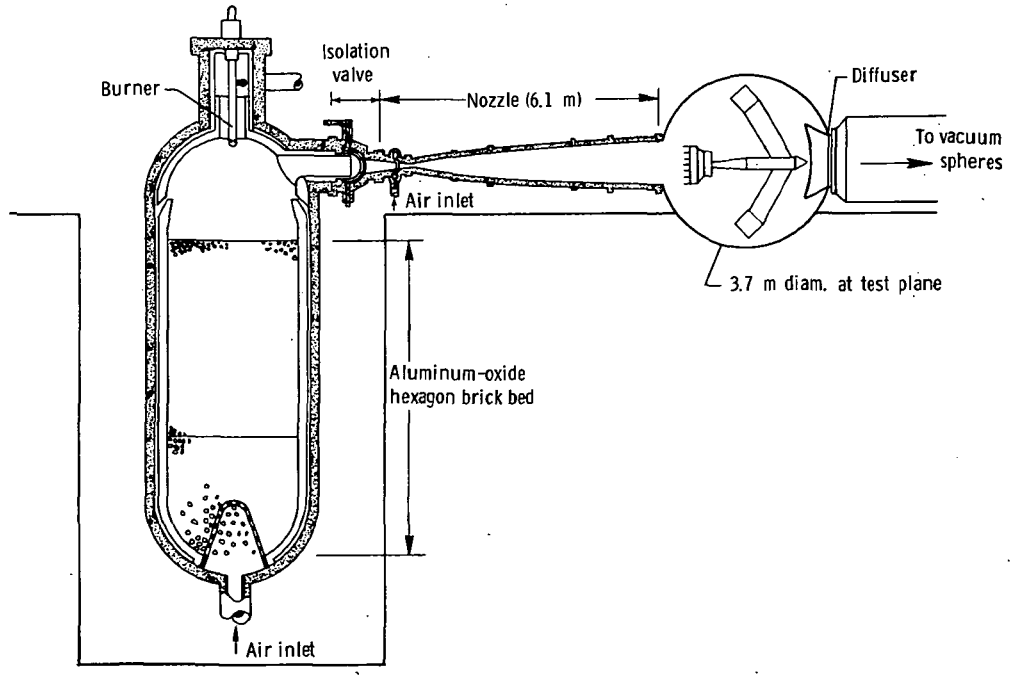

(b) Modification 1 (version B).

Figure 1.- The two versions of the Ames 3.5-foot hypersonic wind tunnel.

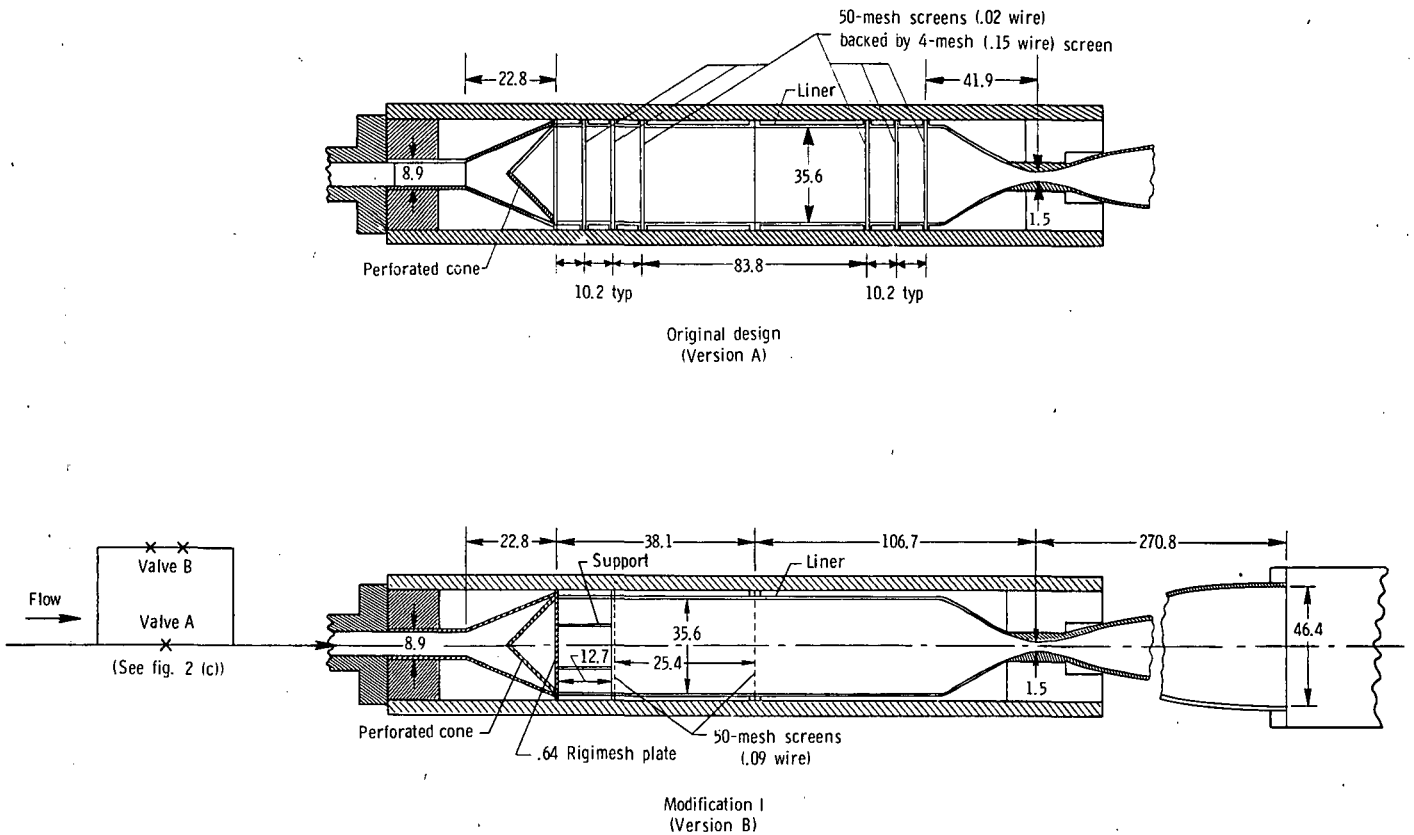

(a) Modifications of settling chamber.

Figure 2.- The Langley Mach 8 variable-density tunnel. Dimensions are in cm.

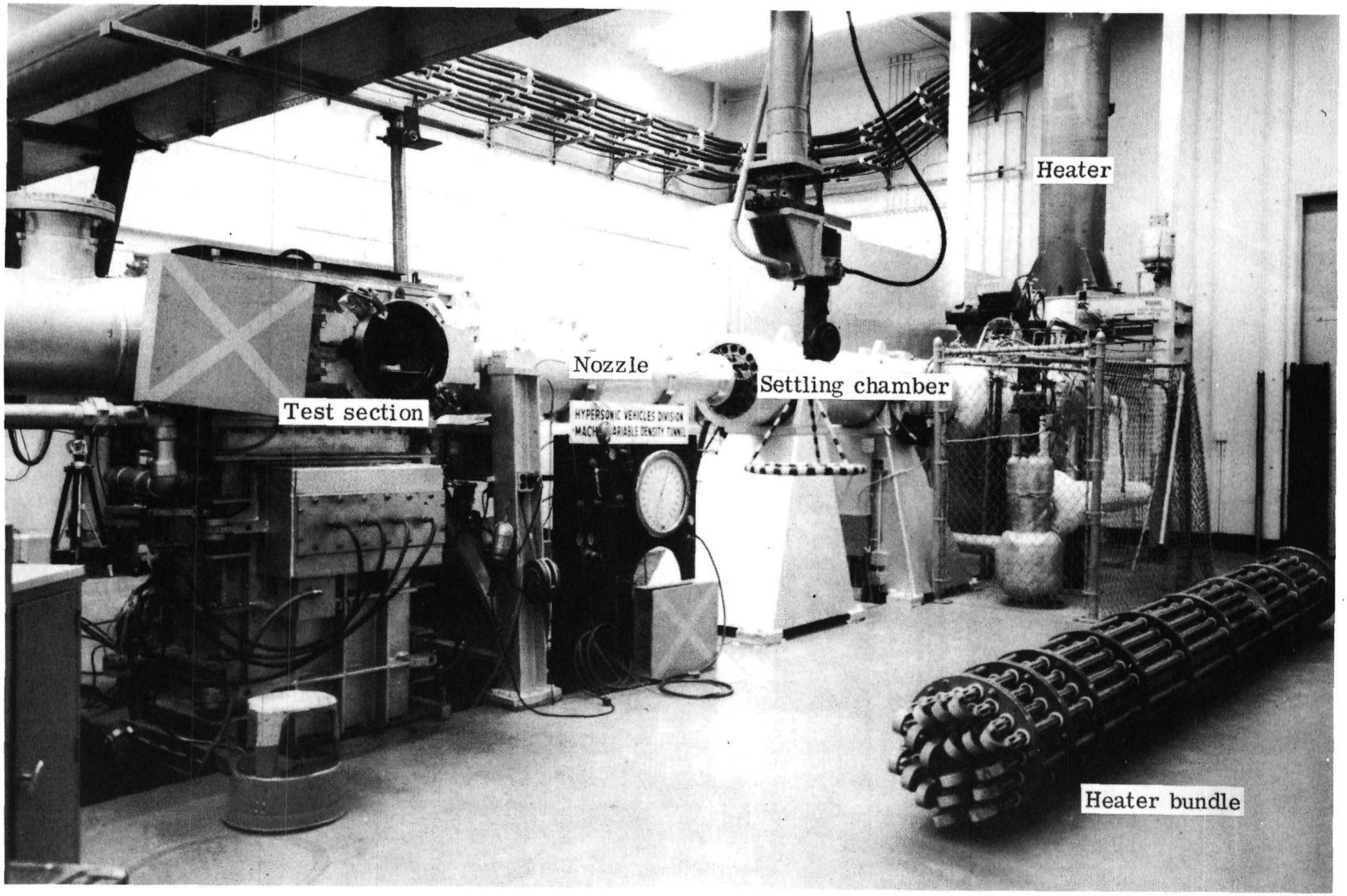

L-73-829.1

(b) General layout of tunnel and heater bundle.

Figure 2.- Continued.

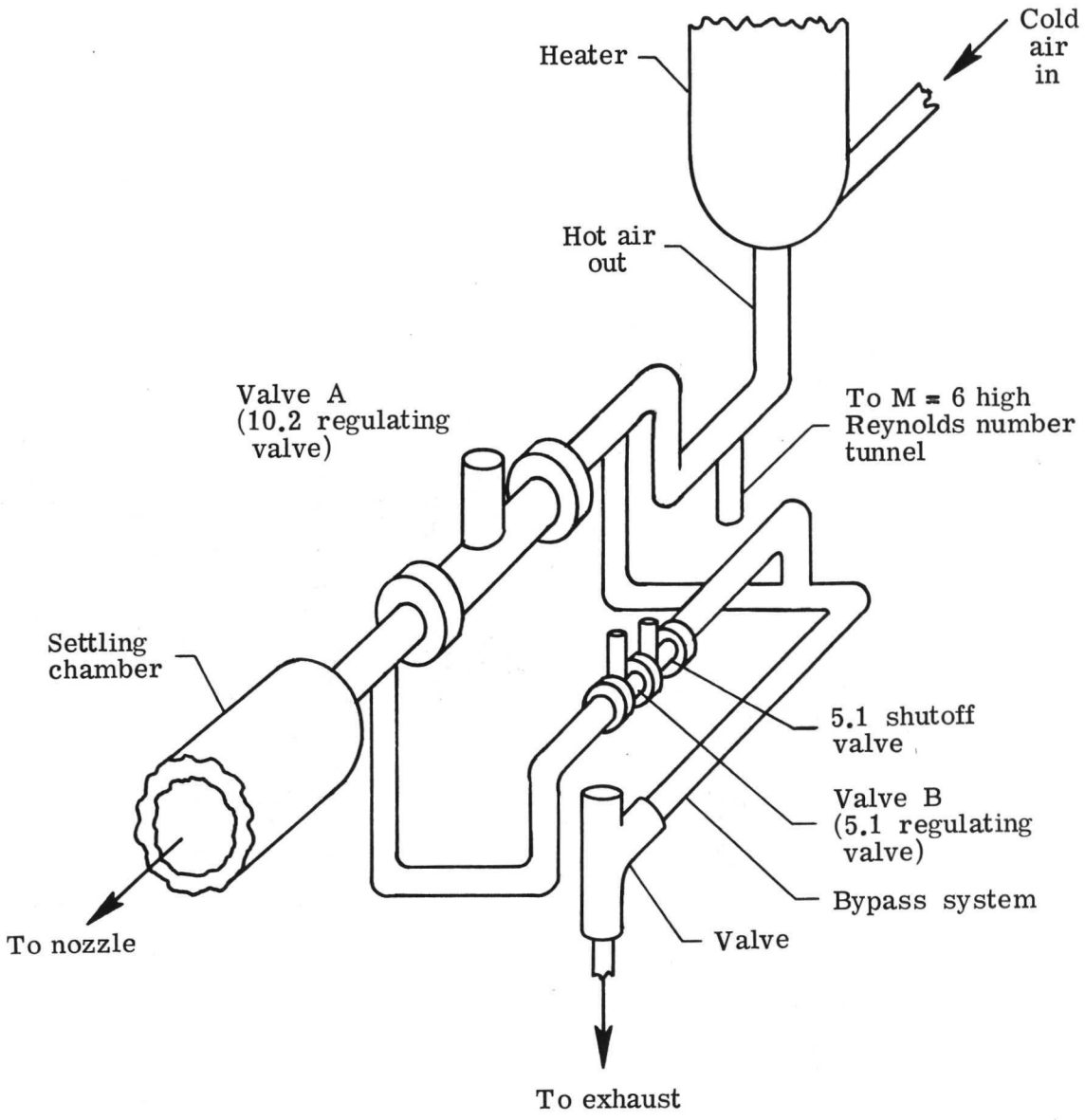

(c) Layout of pipes and valves upstream of settling chamber.

Figure 2.- Concluded.

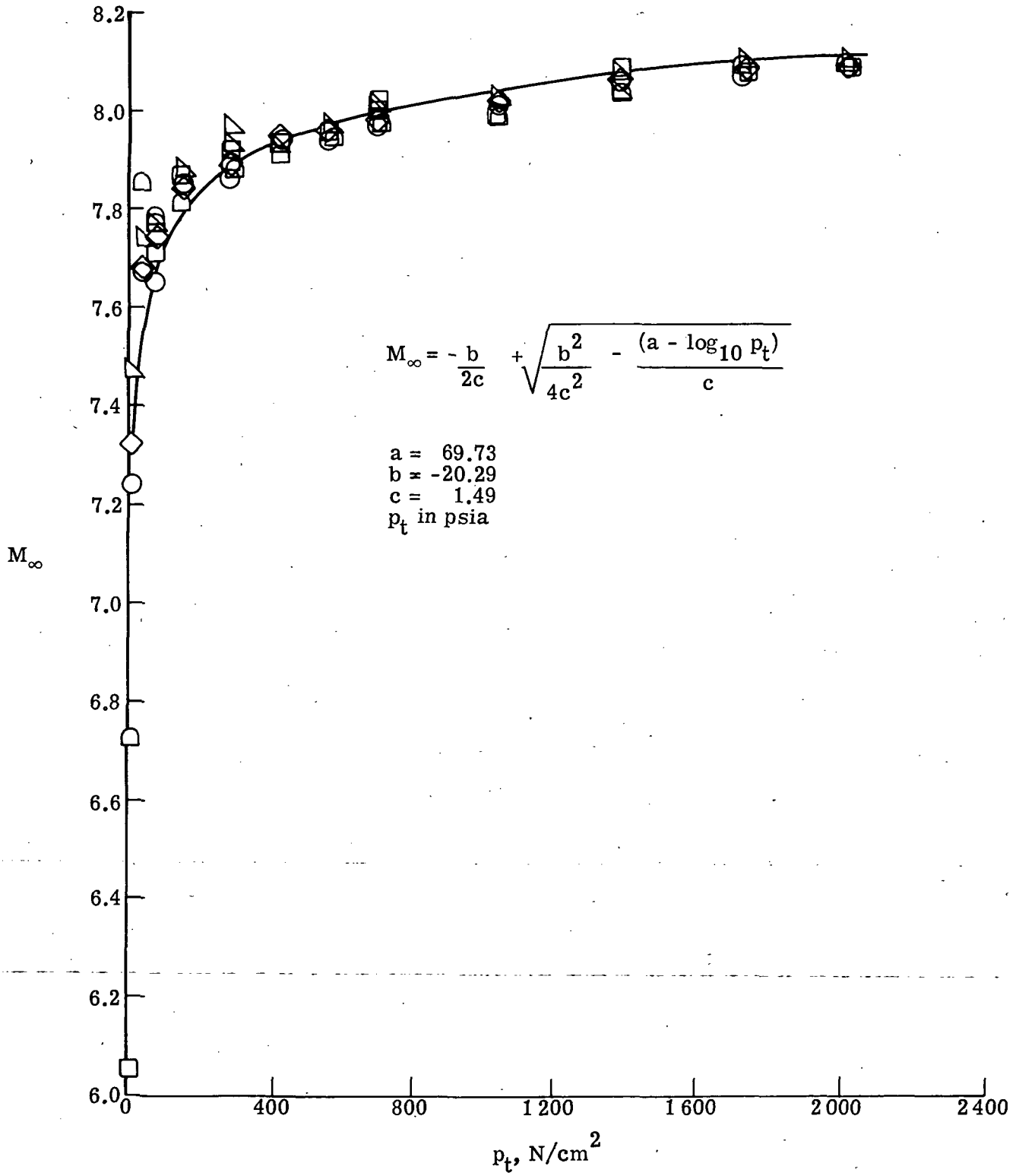

Figure 3.- Calibration for Langley Mach 8 variable-density hypersonic tunnel.

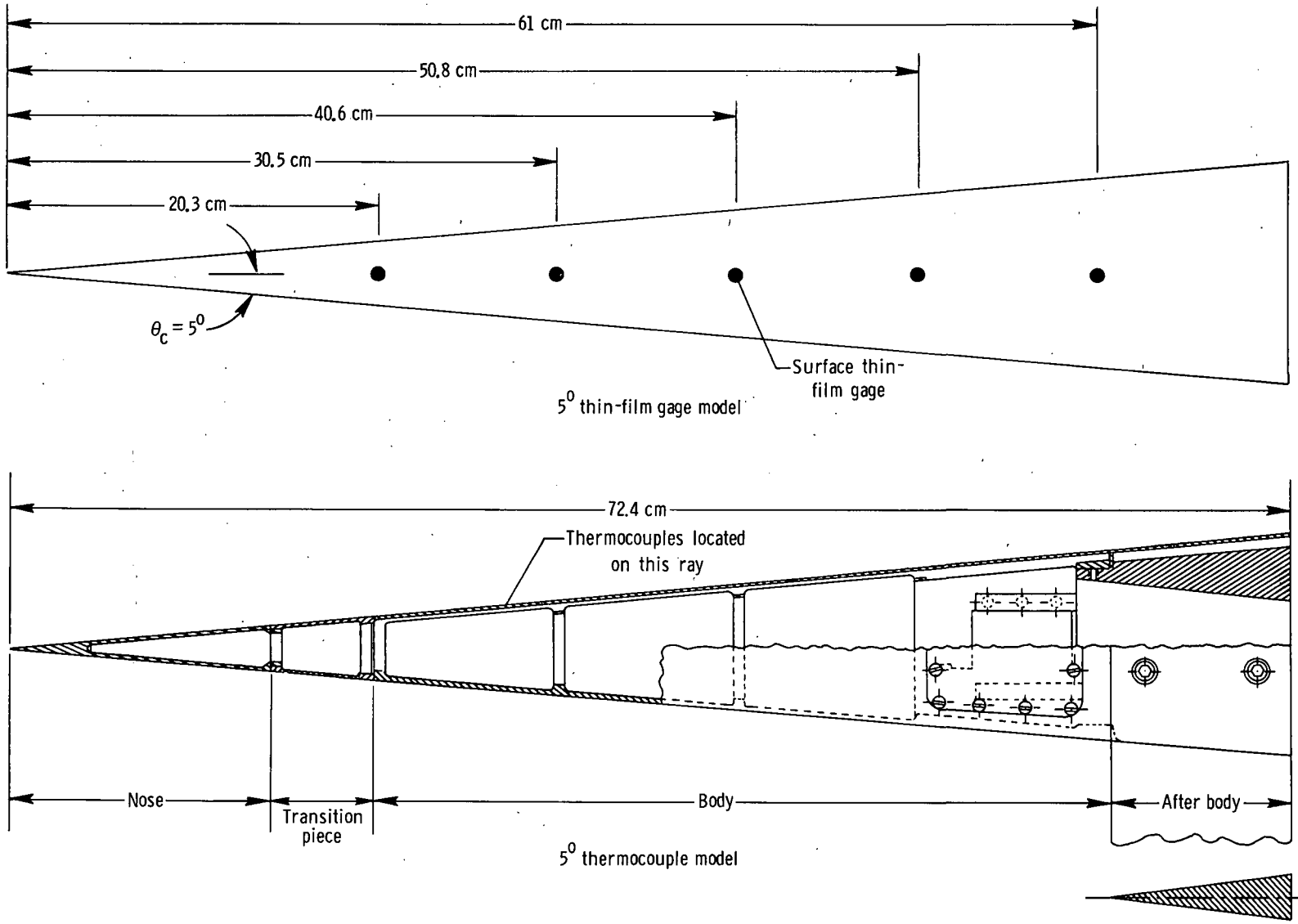

(a) Details of 5^o conical models.

Figure 4.- Models.

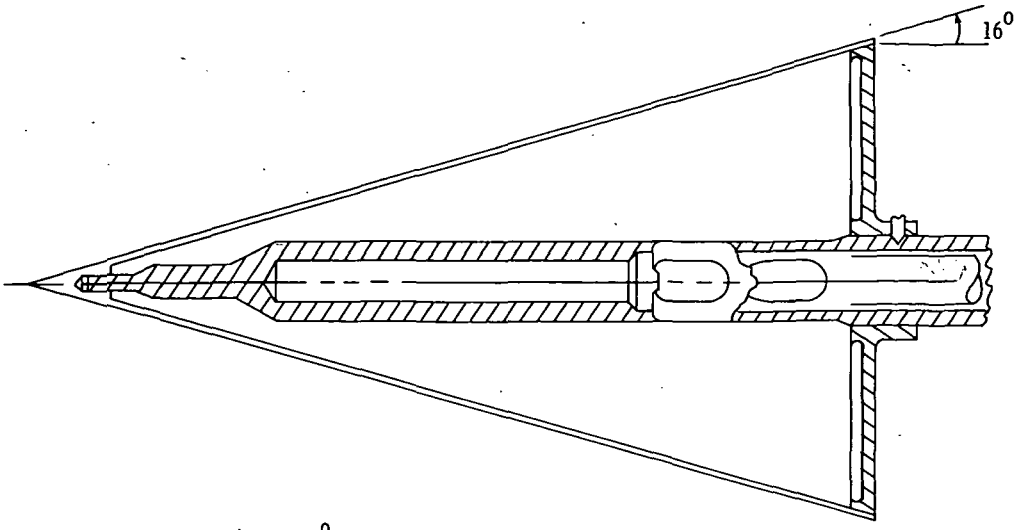

16° thermocouple model (26.6 cm long)

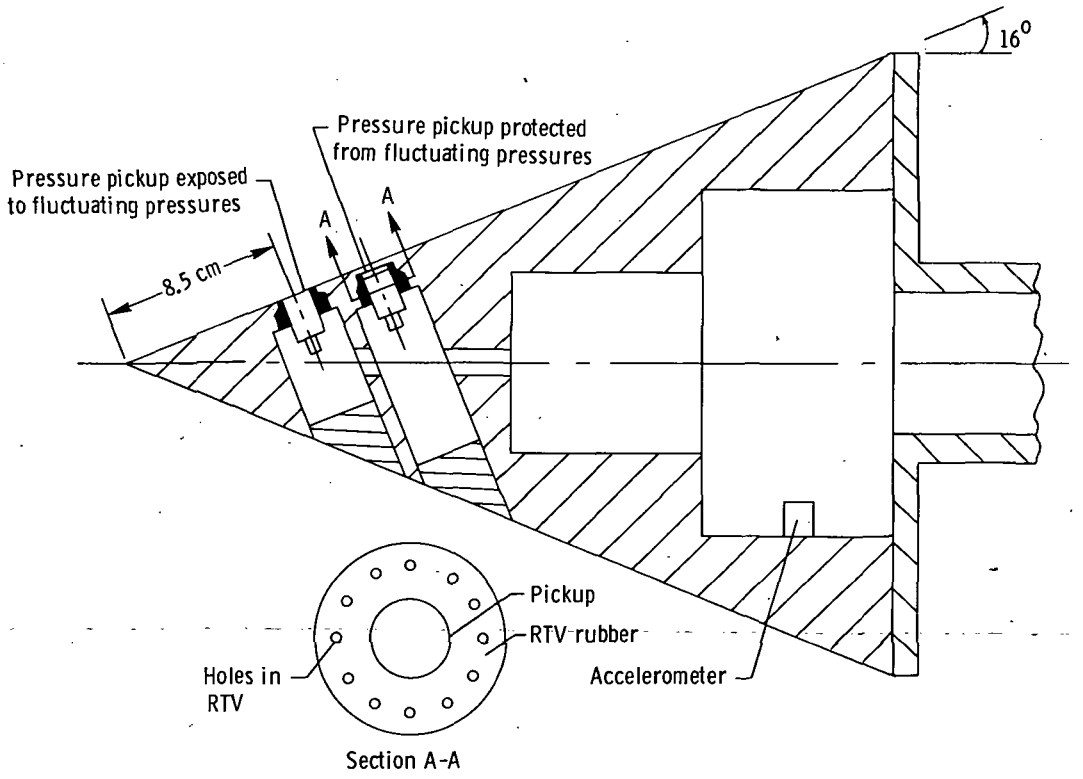

16° pressure model (26.6 cm long)

(b) Details of 16° conical models.

Figure 4.- Concluded.

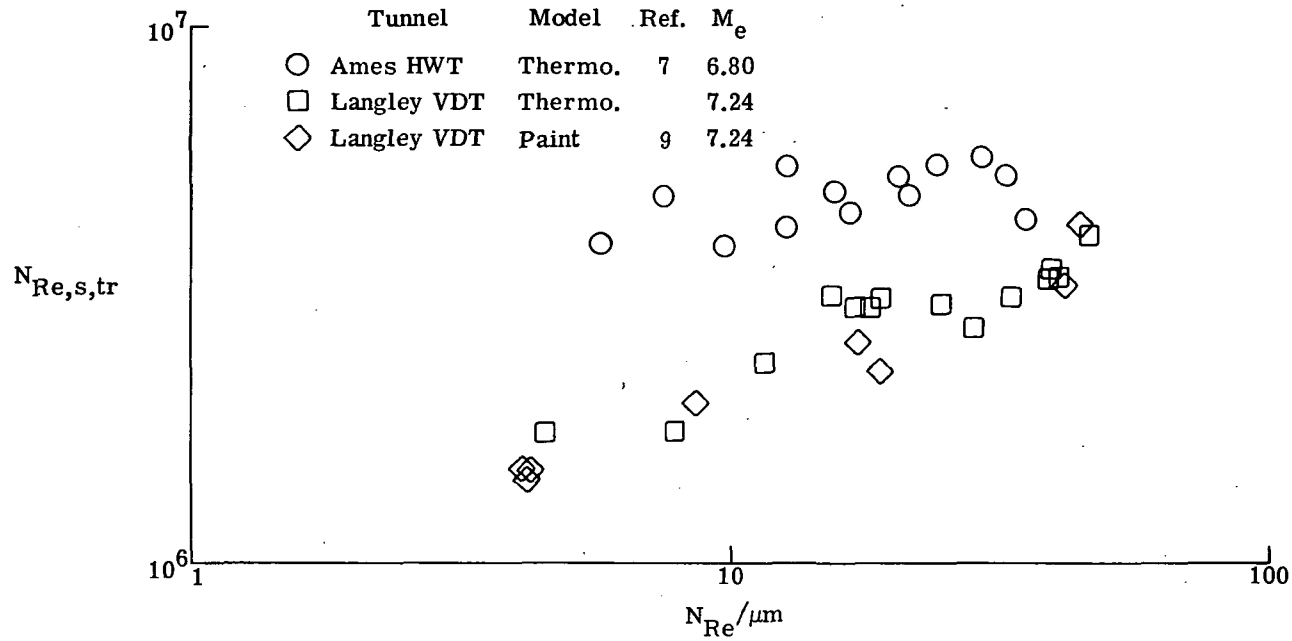

Figure 5.- Transition data from tunnel version A for 5° cone.

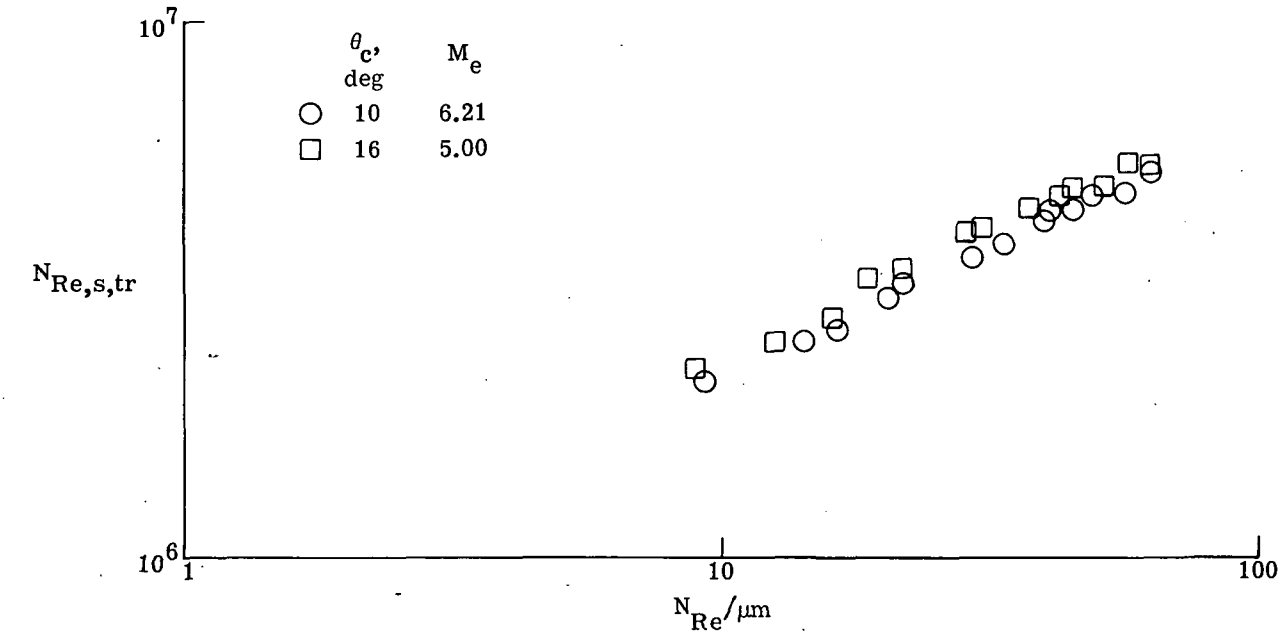

Figure 6.- Transition data from version A of Langley Mach 8 variable-density hypersonic tunnel for thermocouple models.

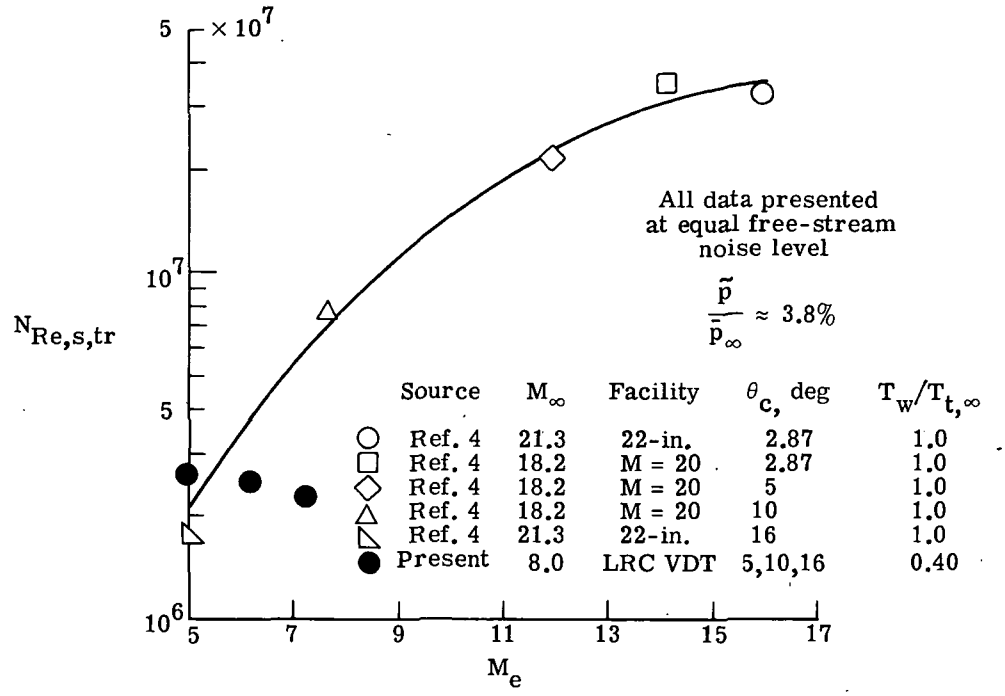

Figure 7.- Effect of local Mach number on cone transition Reynolds number.

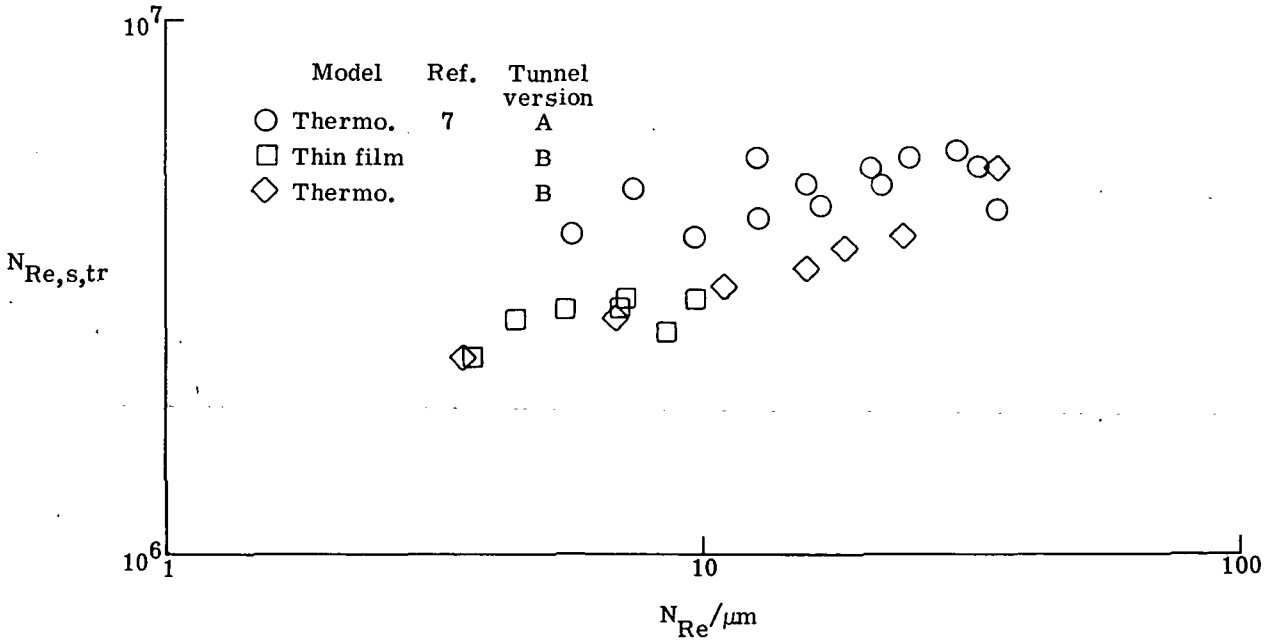

Figure 8.- Transition data for 5° cone taken in Ames 3.5-foot hypersonic wind tunnel.

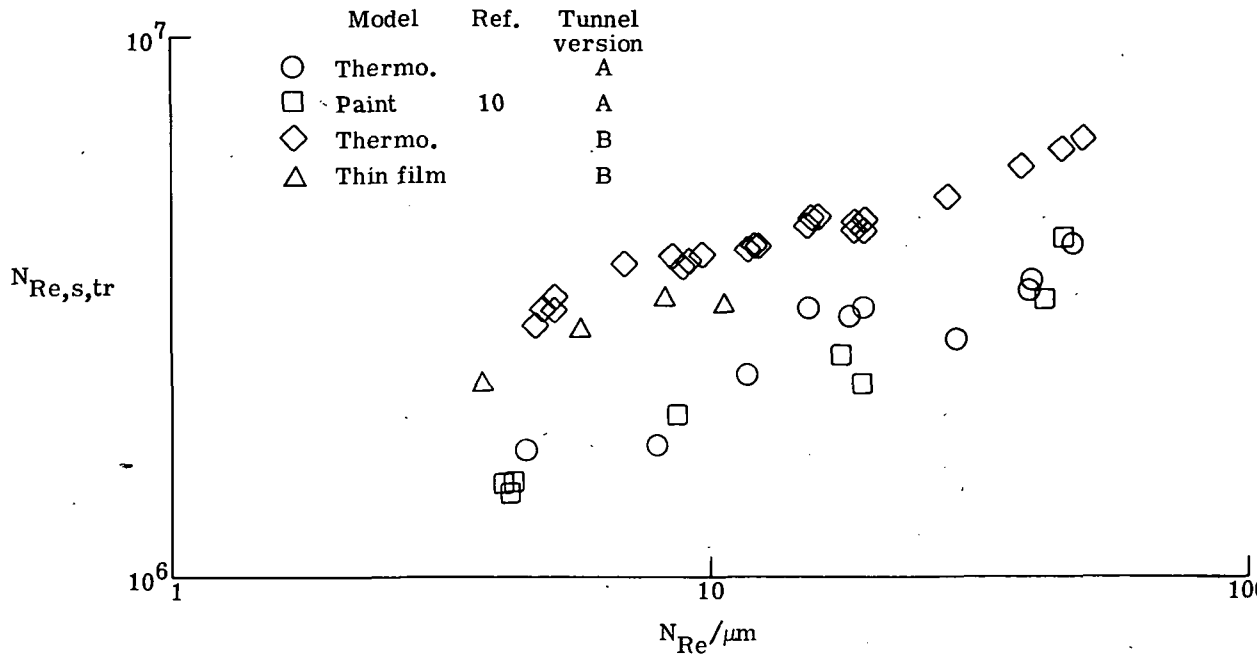

Figure 9.- Transition data for 5° cone taken in Langley Mach 8 variable-density hypersonic tunnel.

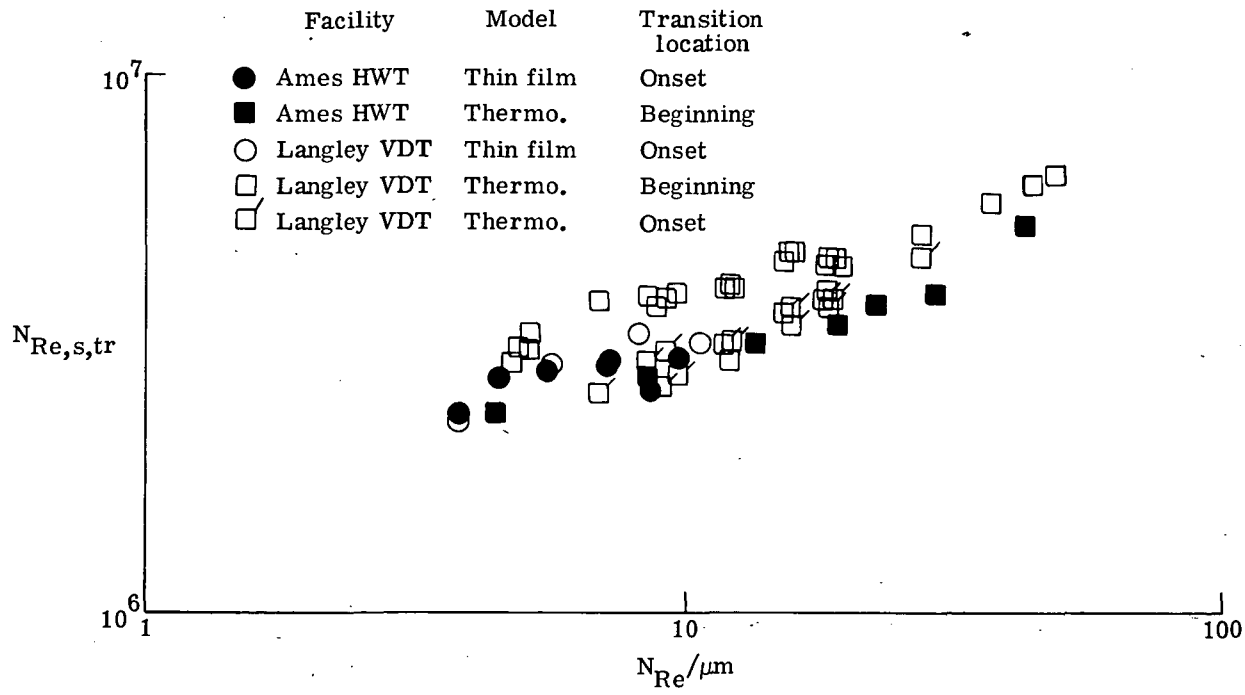

Figure 10.- Comparison of transition data for Ames HWT and Langley VDT. 5° cone; tunnel version B.

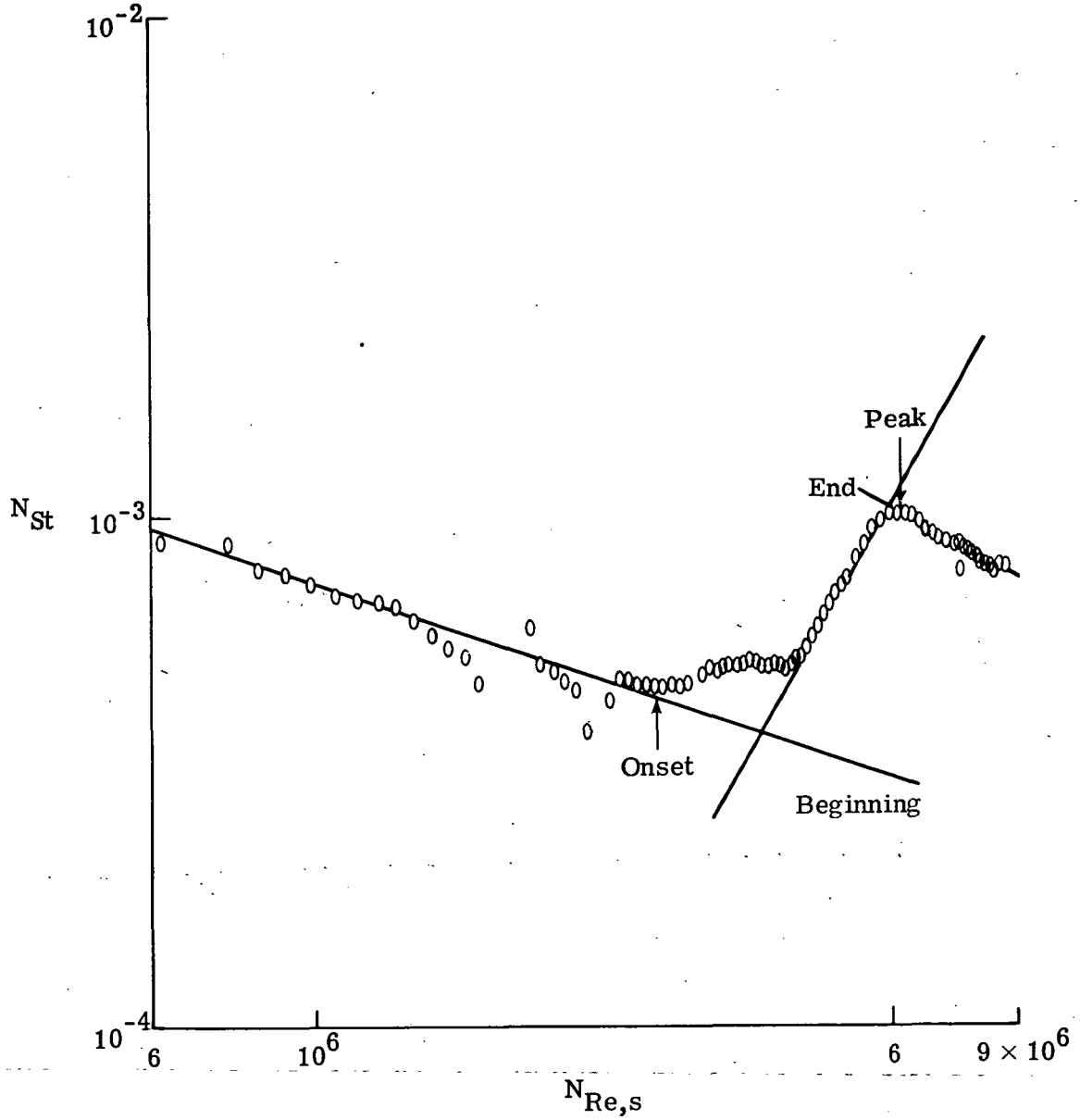

Figure 11.- Example of anomalous heating rate on 5^o cone in Langley VDT.

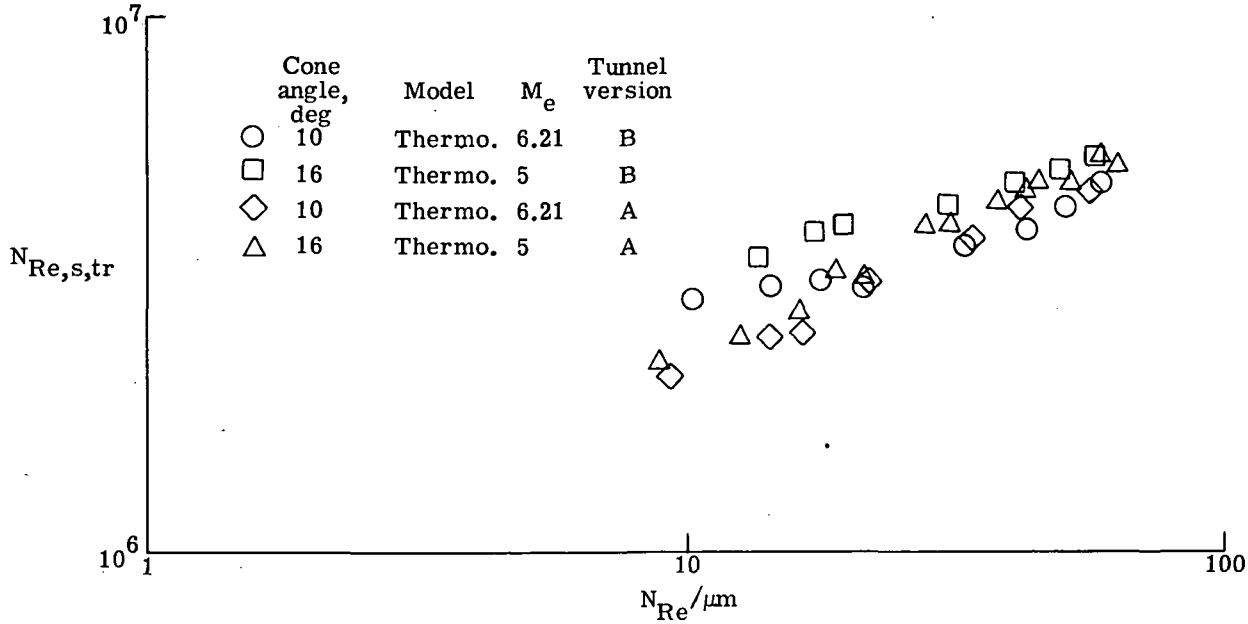

Figure 12.- Transition data for Langley VDT.

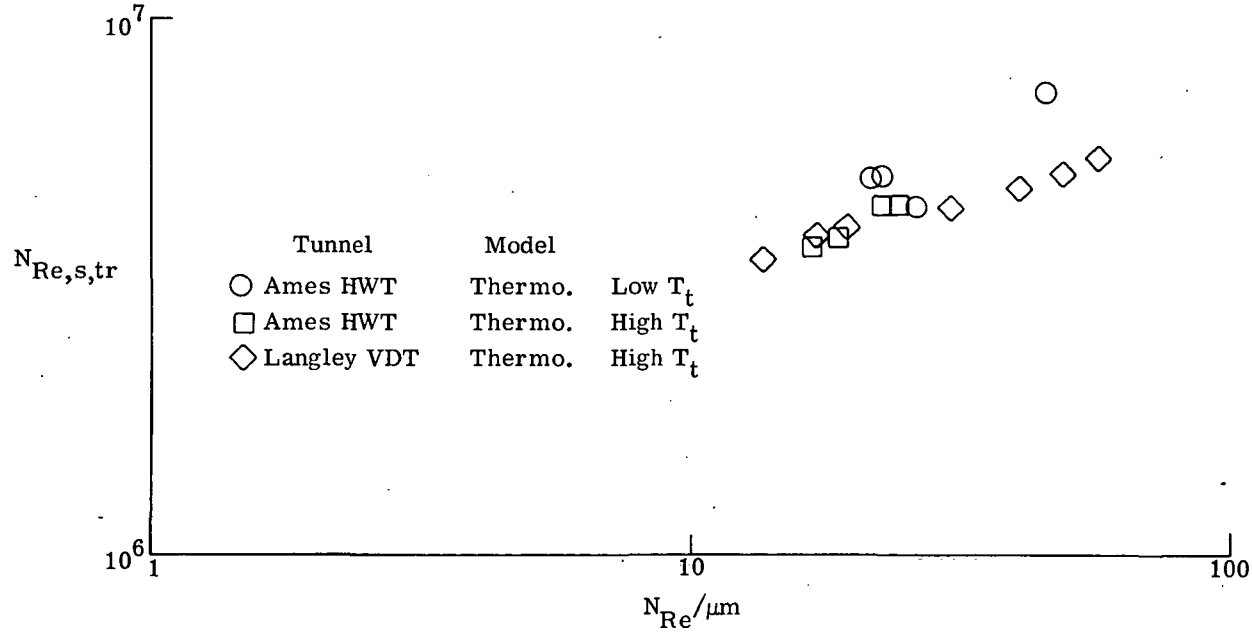

Figure 13.- Transition data for 16° cone. Tunnel version B.

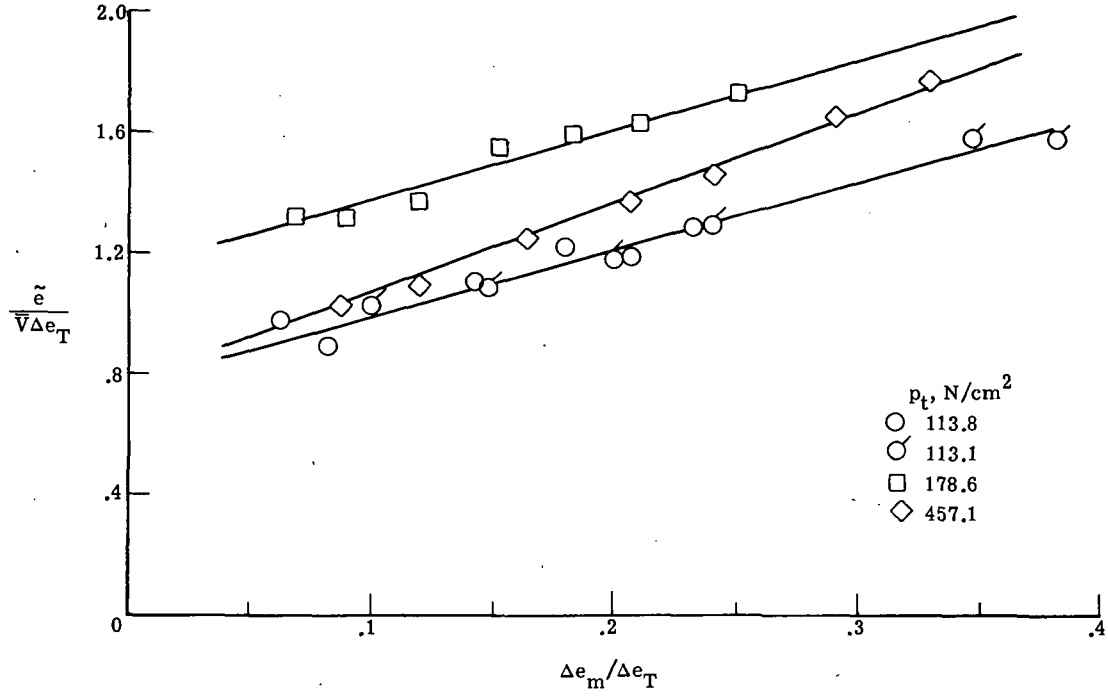

(a) Mode diagram.

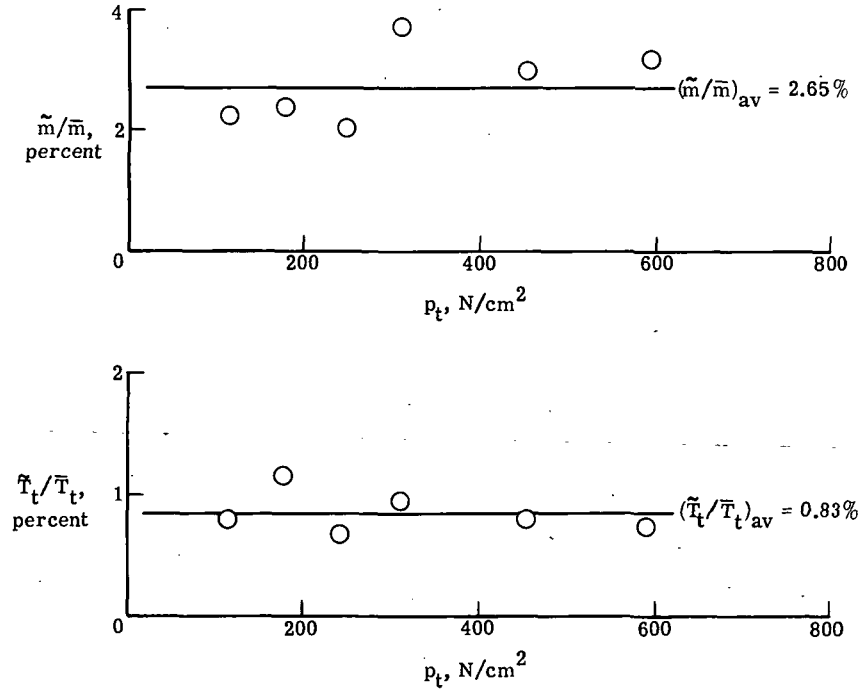

(b) Mass flow and total temperature fluctuations.

Figure 14.- Hot-wire data for Ames HWT.

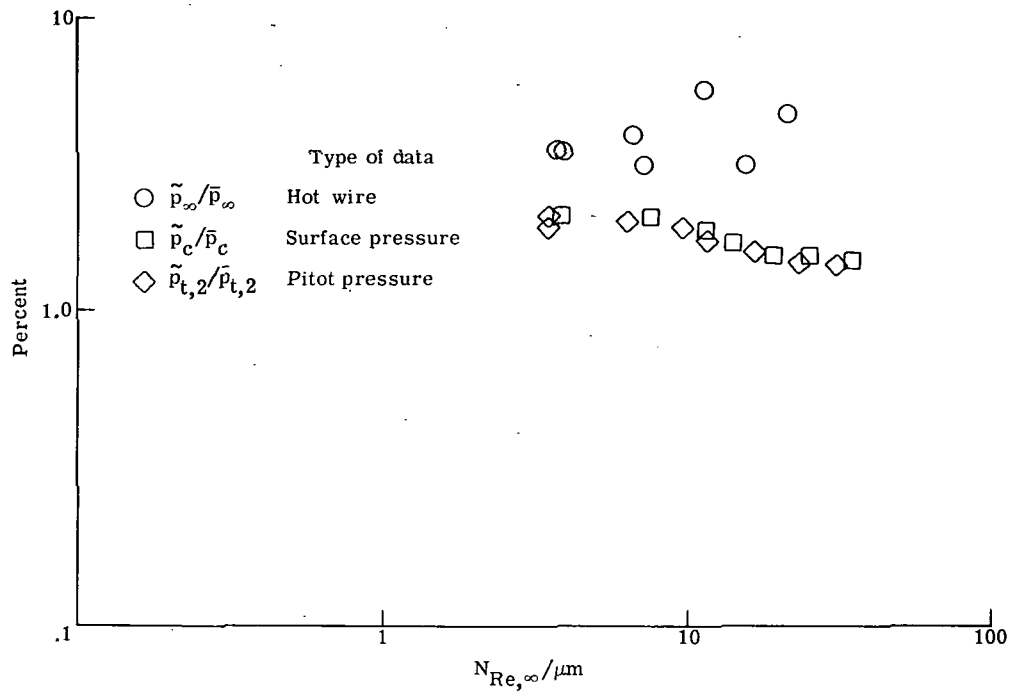

Figure 15.- Disturbance measurements made in Ames HWT.

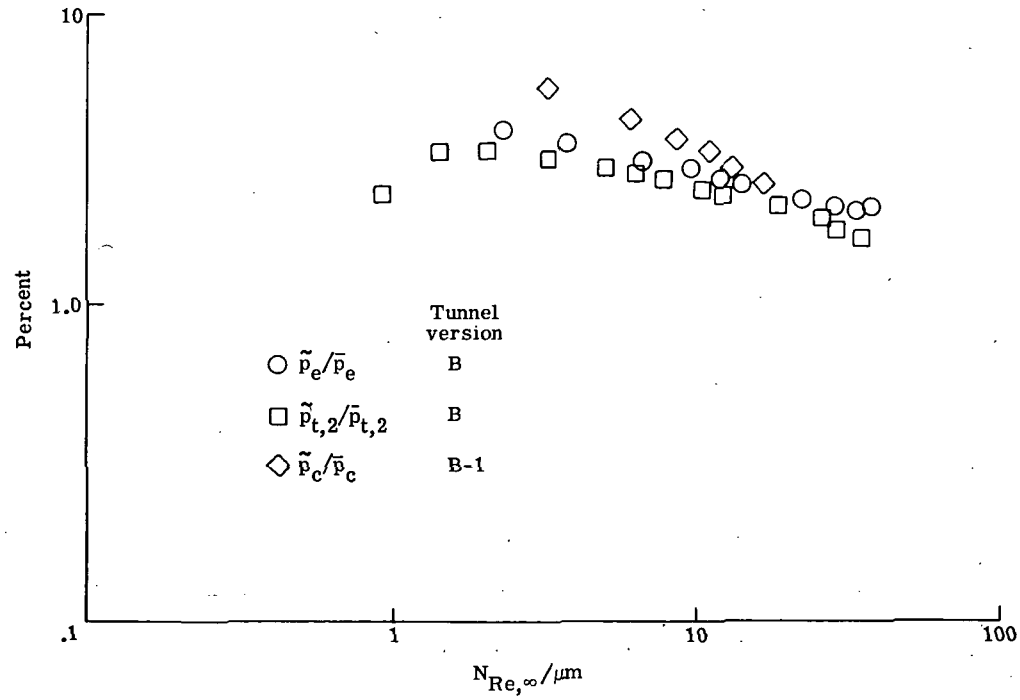

Figure 16.- Disturbance level measurements made in Langley VDT.

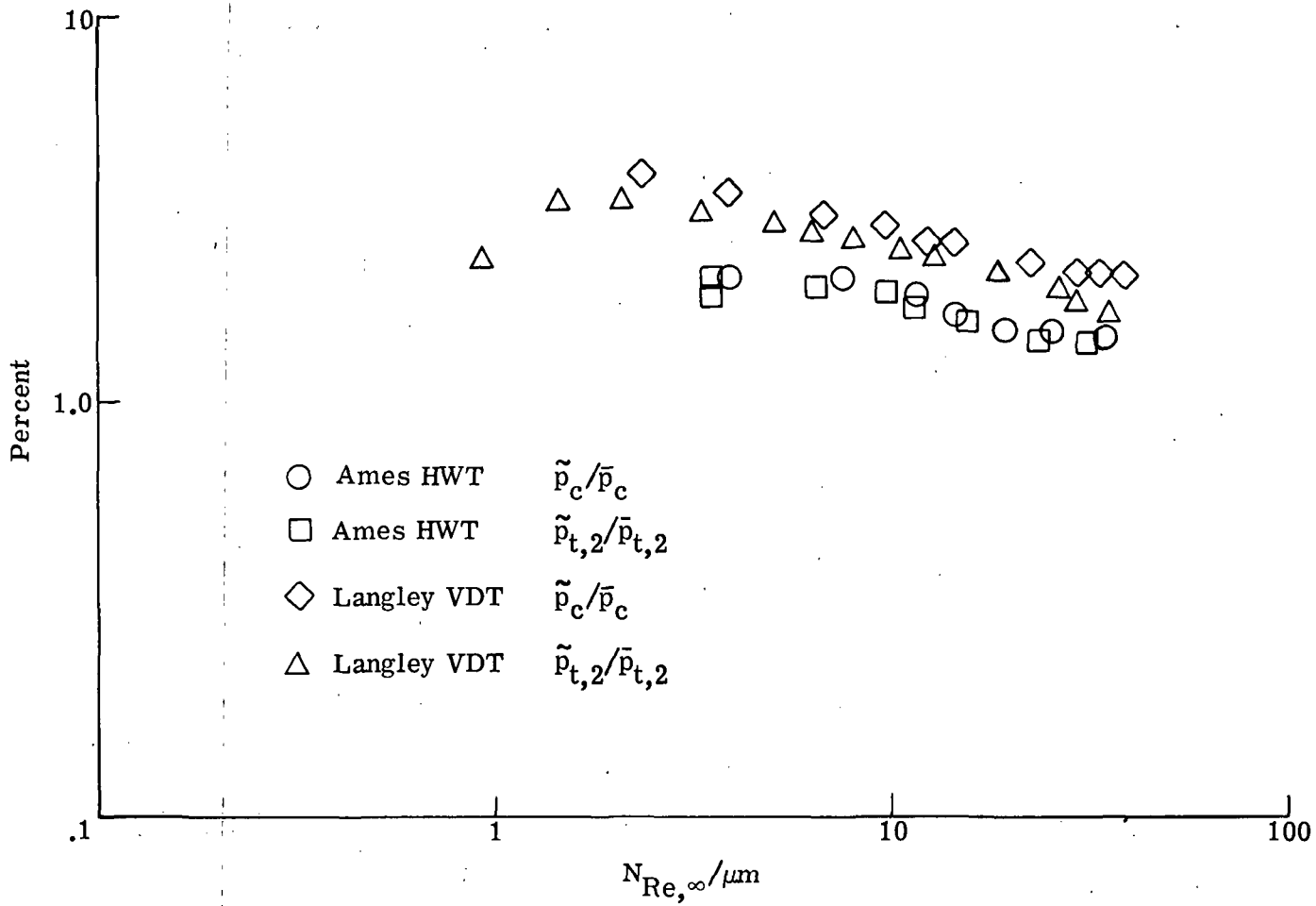

Figure 17.- Disturbance levels measured in the two facilities using pressure transducers. Tunnel version B.

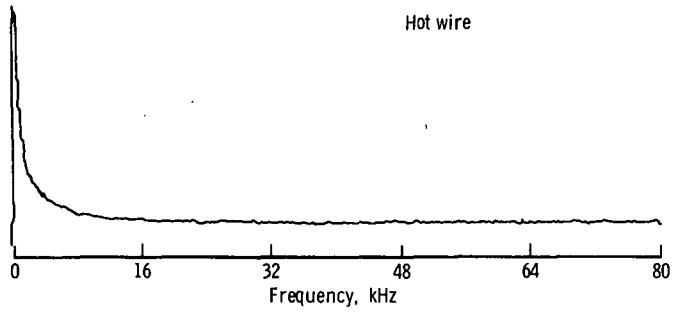

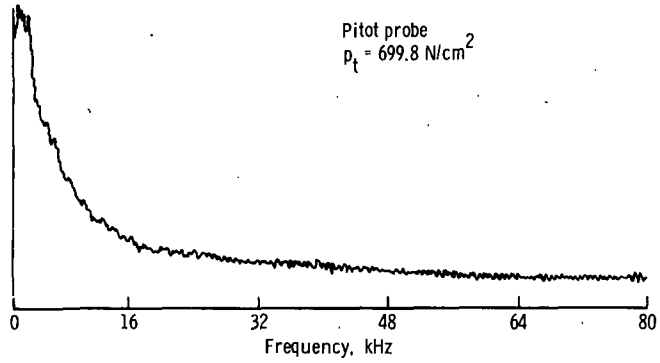

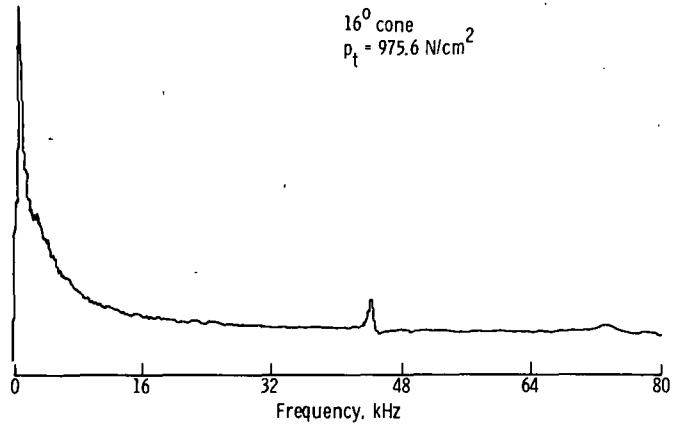

(a) Ames HWT.

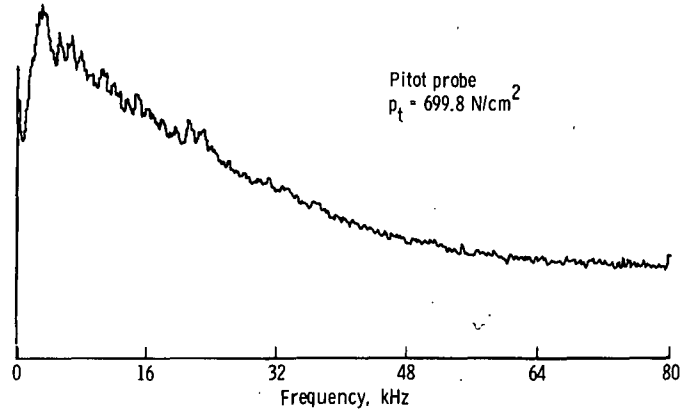

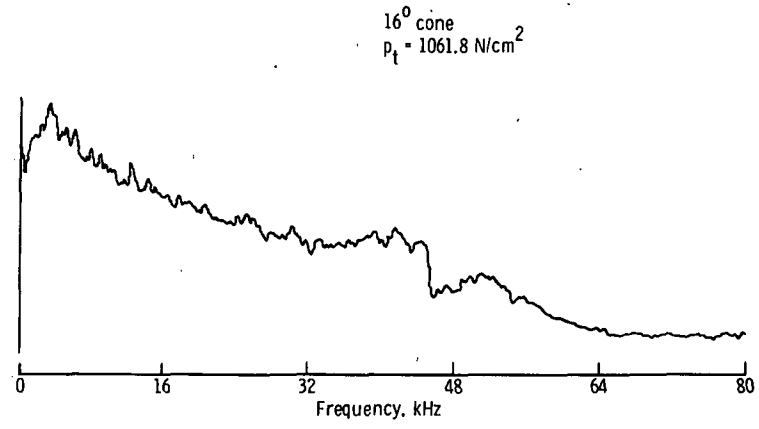

(b) Langley VDT.

Figure 18.- Examples of power density spectra.

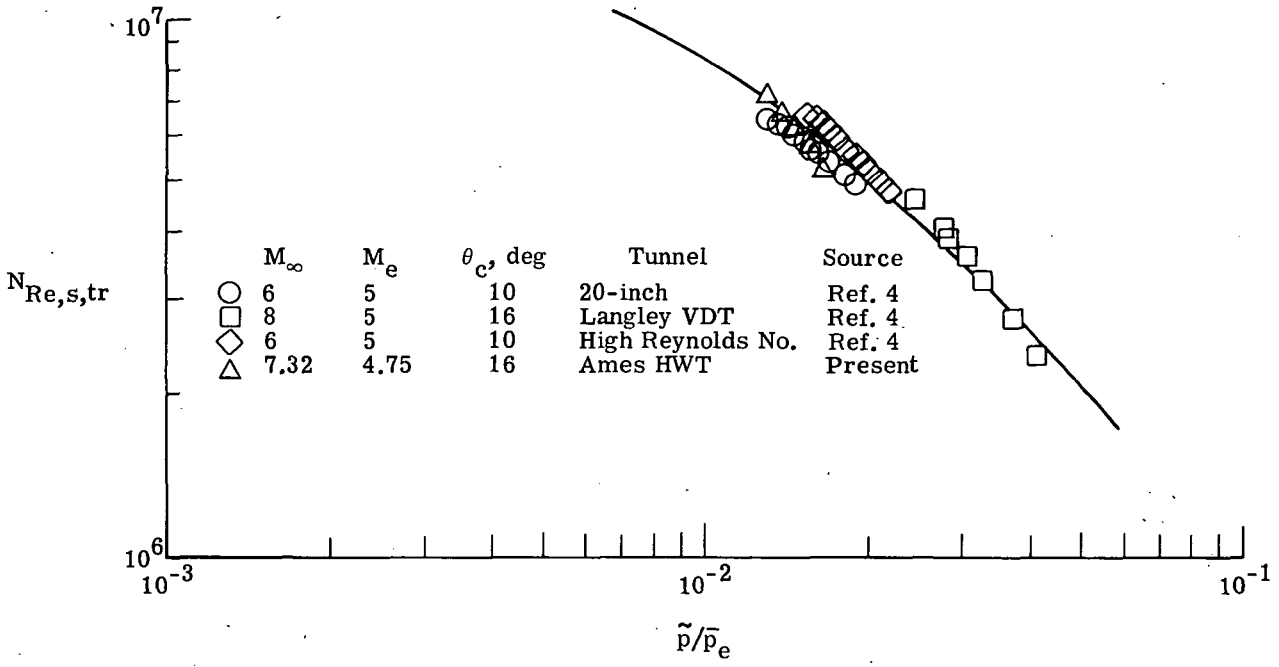

Figure 19.- Correlation of boundary-layer transition with wind-tunnel disturbance intensity.

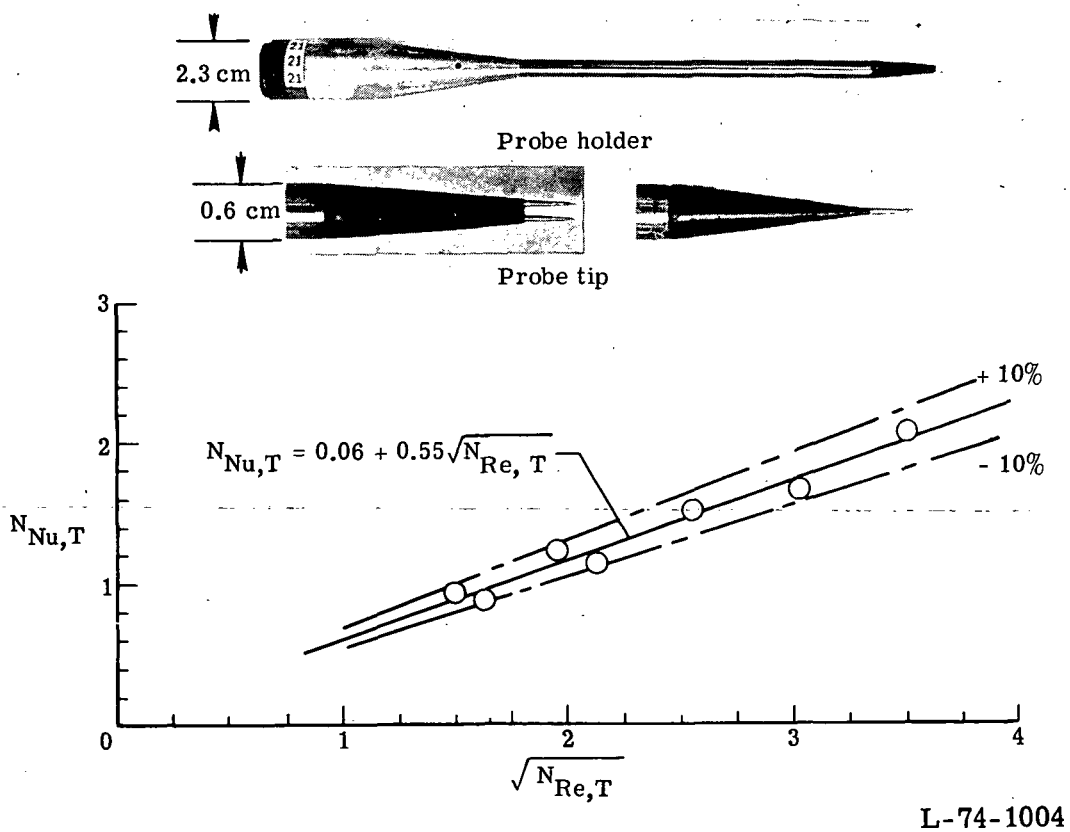

Figure 20.- Wire heat loss calibration.

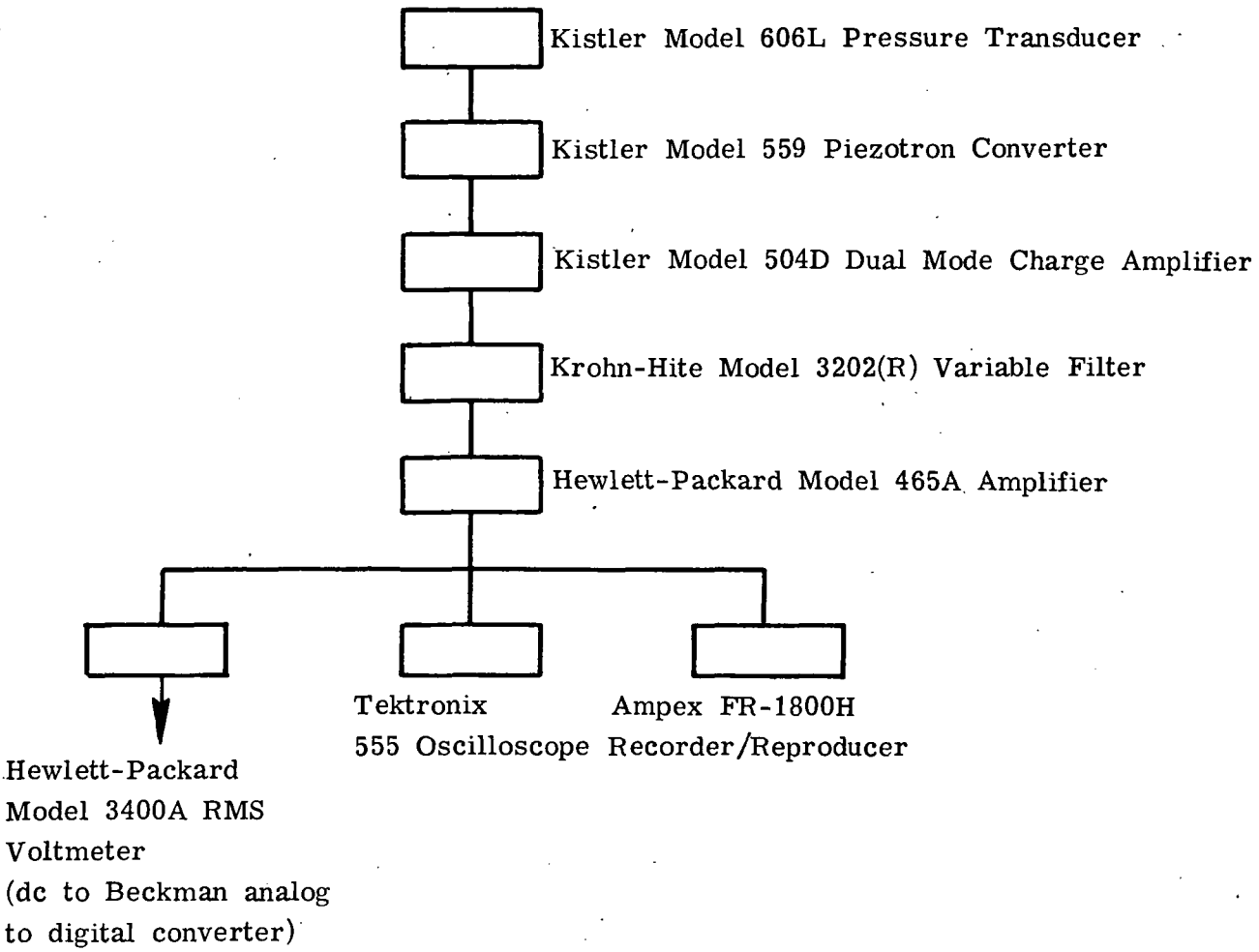

Figure 21.- Schematic diagram of pressure instrumentation.

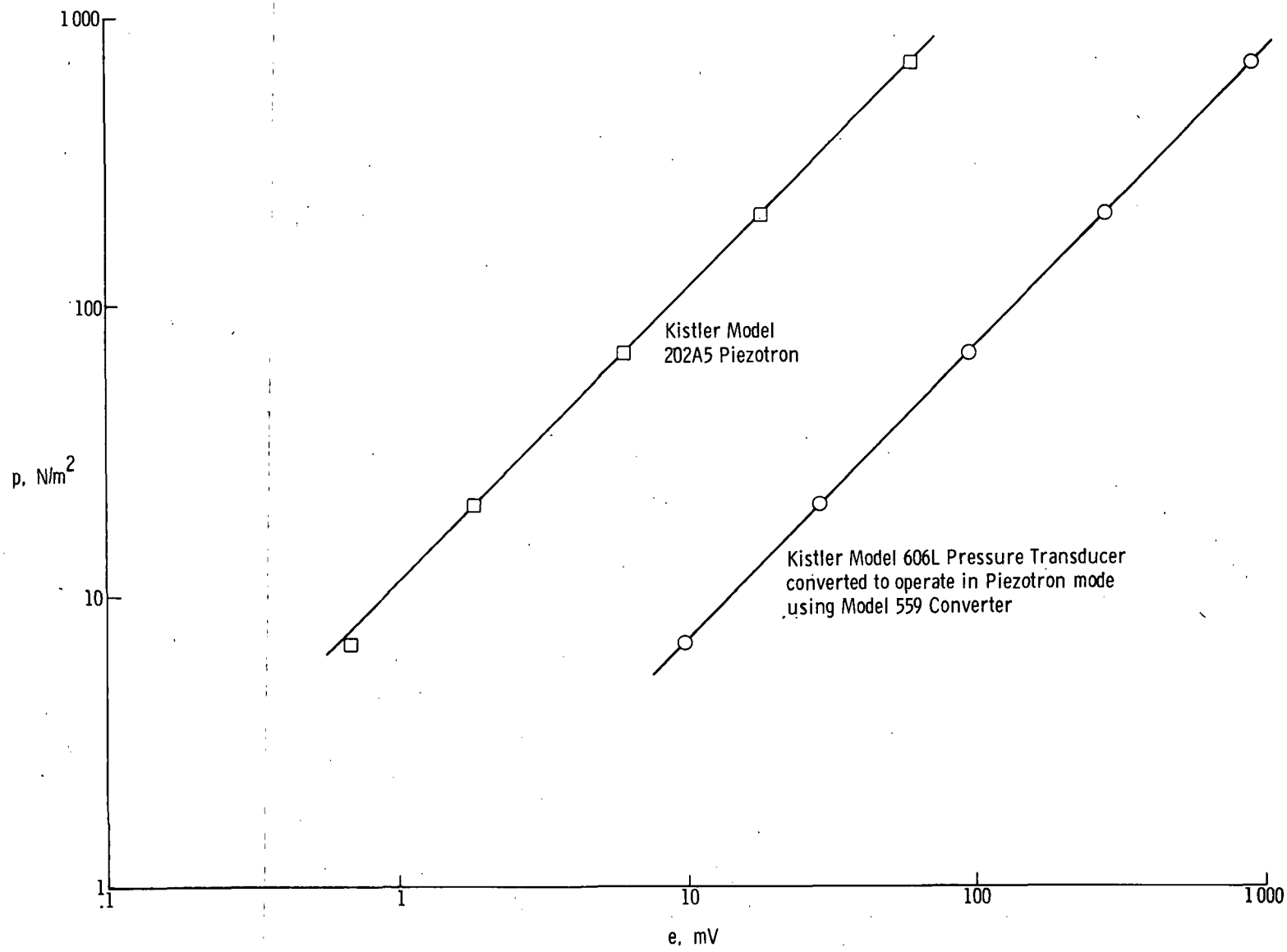

Figure 22.- Calibration of pressure transducers using Photocon Research Products Model PC-120 Pressure Calibrator and Kistler Model 504D Dual Mode Charge Amplifier (range 10).

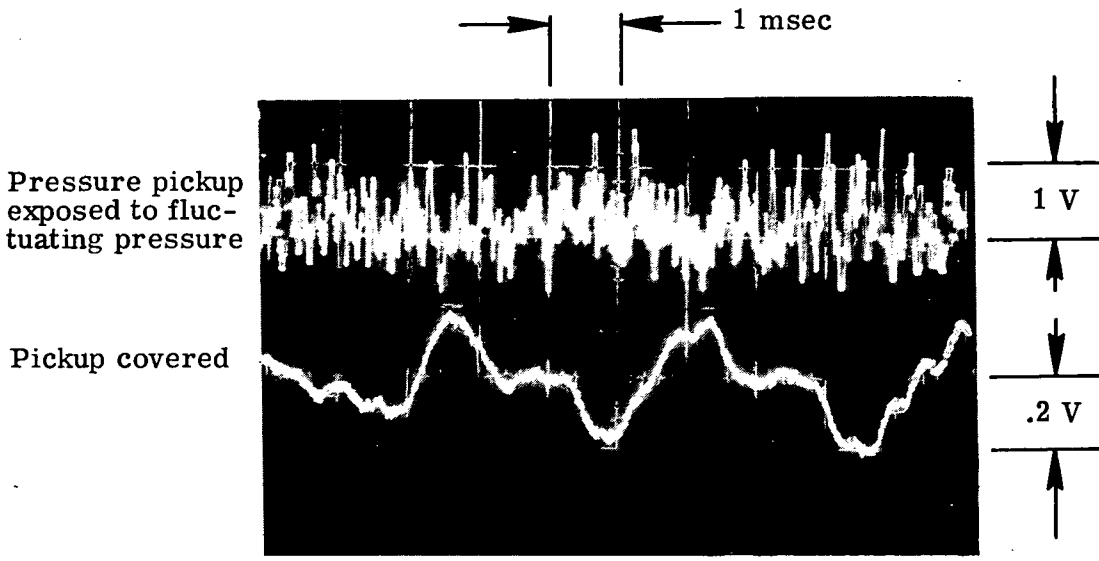

Figure 23.- Example of pressure pickup output.

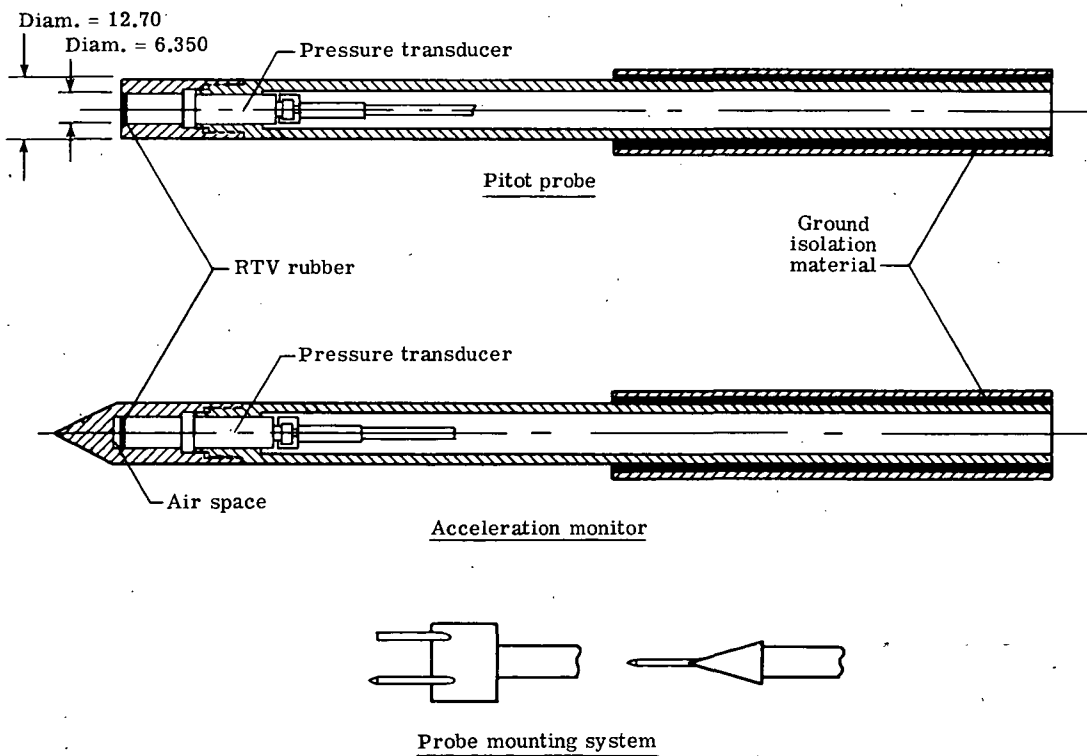

Figure 24.- Method for mounting pressure transducers in pitot probe. Dimensions are in mm.

"The aeronautical and space activities of the United States shall be conducted so as to contribute . . . to the expansion of human knowledge of phenomena in the atmosphere and space. The Administration shall provide for the widest practicable and appropriate dissemination of information concerning its activities and the results thereof."

—NATIONAL AERONAUTICS AND SPACE ACT OF 1958

NASA SCIENTIFIC AND TECHNICAL PUBLICATIONS

TECHNICAL REPORTS: Scientific and technical information considered important, complete, and a lasting contribution to existing knowledge.

TECHNICAL NOTES: Information less broad in scope but nevertheless of importance as a contribution to existing knowledge.

TECHNICAL MEMORANDUMS: Information receiving limited distribution because of preliminary data, security classification, or other reasons. Also includes conference proceedings with either limited or unlimited distribution.

CONTRACTOR REPORTS: Scientific and technical information generated under a NASA contract or grant and considered an important contribution to existing knowledge.

TECHNICAL TRANSLATIONS: Information published in a foreign language considered to merit NASA distribution in English.

SPECIAL PUBLICATIONS: Information derived from or of value to NASA activities. Publications include final reports of major projects, monographs, data compilations, handbooks, sourcebooks, and special bibliographies.

TECHNOLOGY UTILIZATION PUBLICATIONS: Information on technology used by NASA that may be of particular interest in commercial and other non-aerospace applications. Publications include Tech Briefs, Technology Utilization Reports and Technology Surveys.

Details on the availability of these publications may be obtained from:

SCIENTIFIC AND TECHNICAL INFORMATION OFFICE

NATIONAL AERONAUTICS AND SPACE ADMINISTRATION

Washington, D.C. 20546